Acetylcholine Modulates the Precision of Prediction Error in the Auditory Cortex

David Pérez-González[†1,2,3], Ana B. Lao-Rodríguez[†1,2], Cristian Aedo-Sánchez[1,2] & Manuel S. Malmierca[1,2,4*]

[1] Cognitive and Auditory Neuroscience Laboratory, Institute of Neuroscience of Castilla y León, Calle Pintor Fernando Gallego 1, 37007 Salamanca, Spain

[2] Institute for Biomedical Research of Salamanca (IBSAL), 37007 Salamanca, Spain.

[3] Department of Basic Psychology, Psychobiology and Behavioural Science Methodology, Faculty of Psychology, Campus Ciudad Jardín, University of Salamanca, 37005 Salamanca, Spain

[4] Department of Biology and Pathology, Faculty of Medicine, Campus Miguel de Unamuno, University of Salamanca, 37007 Salamanca, Spain

† These authors contributed equally to this work

* Corresponding and leading author: msm@usal.es

ABSTRACT

A fundamental property of sensory systems is their ability to detect novel stimuli in the environment. The auditory brain contains neurons that decrease their response to repetitive sounds but that increase their firing rate to novel or deviant stimuli; the difference between both responses is known as stimulus-specific adaptation or neuronal mismatch (nMM). Here, we tested the effect of microiontophoretic applications of ACh on the neuronal responses in the auditory cortex (AC) of anesthetized rats during an auditory oddball paradigm, including cascade controls. Results indicate that ACh modulates the nMM, affecting prediction error responses but not repetition suppression, and this effect is manifest predominantly in infragranular cortical layers. The differential effect of ACh on responses to standards, relative to deviants (in terms of averages and variances), were consistent with the representational sharpening that accompanies an increase in the precision of prediction errors. These findings suggest that ACh plays an important role in modulating prediction error signaling in the AC and gating the access of these signals to higher cognitive levels.

INTRODUCTION

Neuromodulation strongly impacts sensory processing by influencing neuronal excitability or synaptic processes in neuronal circuits (Hasselmo and Giocomo, 2006; Lucas-Meunier et al., 2003; Metherate, 2011; Muñoz and Rudy, 2014; Picciotto et al., 2012). Acetylcholine (ACh) is a widely distributed neuromodulator throughout the brain, including the auditory cortex (AC), and modulates processes such as attention, learning, memory, arousal, sleep and/or cognitive reinforcement (Batista-Brito et al., 2018; Dalley et al., 2004; Franklin and Frank, 2015). The main source of ACh to the AC is the basal forebrain (Chavez and Zaborszky, 2017; Mesulam, 2013; Zaborszky et al., 2008). In the auditory system, cholinergic modulation is known to alter frequency response areas generating changes across frequency tuning, decreasing the acoustic threshold at the characteristic frequency and changing the encoding of spectral representation of many auditory neurons (Ma and Suga, 2005; Metherate, 2011) Thus, ACh promotes neuronal and synaptic plasticity at different temporal scales (Kamke et al., 2005; Kilgard and Merzenich, 1998).

Here, we characterized the effect of ACh on stimulus-specific adaptation (SSA), a type of neuronal adaptation found in the AC. SSA is elicited by an oddball paradigm, which comprises a pattern of repeating sounds (standards), interrupted by a low-probability and unexpected sound (deviant). The deviant usually differs in frequency, but could differ on any other physical dimension from the standard, or otherwise violate a pattern of regularity established by the standard (Chen et al., 2015; Nieto-Diego and Malmierca, 2016; Parras et al., 2017; Ulanovsky et al., 2003; von der Behrens et al., 2009).

Thus, neurons that exhibit SSA adapt specifically to the standard stimulus but resume their firing when a deviant stimulus appears. SSA has been proposed to be a neuronal correlate of 'mismatch negativity' (MMN), an evoked potential obtained in human and animal electroencephalographic studies using the oddball paradigm (Nieto-Diego and Malmierca, 2016; Ulanovsky et al., 2003). Hence, SSA has been also referred to as neuronal mismatch (nMM) in animal models (Casado-Román et al., 2020; Lao-Rodríguez et al., 2023; Parras et al., 2020, 2017), a nomenclature that highlights deviance detection, as well as other underlying processes other than neuronal adaptation. Because nMM is considered a form of short-term plasticity (Ogawa and Oka, 2015) and ACh has been shown to play a role in this type of neural plasticity (Marshall et al., 2016; Moran et al., 2013; Parr and Friston, 2017; Vossel et al., 2012) it is plausible that ACh may be involved in the generation and/or modulation of nMM. Furthermore, it has been shown that ACh differentially modulates the neural response to the standard stimulus in units of the IC (Ayala and Malmierca, 2015).

Currently, MMN and nMM are best explained by the predictive coding theory (Friston, 2008, 2005). According to the predictive coding framework, higher-level cortical areas generate predictions about sensory streams that are conveyed in a top-down manner to lower hierarchical levels, to suppress the ascending neuronal activity evoked by sensory events that can be anticipated. However, when current predictions do not match the sensory inputs, then the lower levels send forward bottom-up prediction errors to higher hierarchical levels (Friston and Kiebel, 2009).

In the setting of an oddball paradigm, every evoked response is considered to be a prediction error response. When the stimulus does not change, sensory learning enables better predictions to progressively attenuate the response to standards until an oddball or deviant stimulus is encountered — and a large prediction error is seen. The prediction

error response to oddball stimuli may be further augmented by increasing the precision or gain of prediction errors: predictive coding models weigh sensory prediction errors by their precision, which is the inverse of variance. Precision weighting of prediction errors therefore encodes the confidence afforded information (i.e., prediction errors) in terms of their signal-to-noise ratio (Parr and Friston, 2017). In neurobiological terms, precision has been suggested to be mediated by synaptic gain modulation; namely, the sensitivity of postsynaptic responses to neural inputs (Adams et al., 2021) and is likely implemented by cholinergic neuromodulation (Moran et al., 2013; Yu and Dayan, 2005, 2002). Increasing the gain of certain neuronal populations — e.g., superficial pyramidal cells reporting prediction errors – affords them privileged access to higher levels of processing and ensuing Bayesian belief updating. This can be likened to attentional gain in psychological terms – or increasing the Kalman gain in terms of Bayesian filtering.

According to the predictive coding model there are therefore two mechanisms underlying the MMN/nMM (Auksztulewicz and Friston, 2016; Carbajal and Malmierca, 2018; Friston, 2008; Harms et al., 2020; Parras et al., 2017). First, nMM could reflect the repetition suppression (RS) of the response to the predictable stimuli (standards) due to sensory learning – that resolves sensory prediction errors as predictions become more accurate. In addition, nMM could also reflect an increase in the precision or gain afforded prediction errors, when the (oddball) stimulus cannot be predicted; enabling the ascending prediction errors to revise higher level representations about the auditory stream. In short, oddball stimuli elicit an enhanced neural response when an unexpected (deviant) stimulus is presented. Repetition suppression and prediction error modulation can be distinguished using control sequences (Ruhnau et al., 2012), and there is now evidence in both humans and rodents that MMN/nMM receives contributions from both

110 prediction error (modulation) and repetition suppression (sensory learning) at various
111 levels of the auditory system (Ishishita et al., 2019; Parras et al., 2017).

112 The main goal of the present study was to determine the role that ACh plays in the
113 modulation of prediction errors and repetition suppression in the rat AC; utilizing
114 control sequences to disambiguate these mechanisms (Nieto-Diego and Malmierca,
115 2016; Parras et al., 2017). We used microiontophoretic injections of ACh, to determine
116 how ACh neurotransmission affects the responses of AC neurons that exhibit nMM, to
117 establish the role of ACh on prediction error modulation and repetition suppression, in
118 both primary and secondary AC areas.

119

120 **RESULTS**

121 To explore the influence of cholinergic modulation on nMM, we recorded a total of 113 units
122 in the AC before, during and after the microiontophoretic injection of acetylcholine.
123 Recording depths ranged 120–1191 μm including neurons from all layers.

124 To allocate each recorded neuron to a specific field in the AC, we recorded the frequency
125 response area (FRA) and analyzed the topographical distribution of CF (characteristic
126 frequency) for each unit. Each recording was assigned to a dorsoventral and rostrocaudal
127 coordinate system relative to bregma as in previous studies (Nieto-Diego and Malmierca,
128 2016; Parras et al., 2017; Polley et al., 2007). This analysis allowed us to pool the data from
129 all animals (Fig. 1a) and construct a synthetic map of the CF across the entire rat auditory
130 cortex (Nieto-Diego and Malmierca, 2016; Parras et al., 2017). Similar to these previous
131 studies, we found a high-frequency reversal zone between ventral auditory field (VAF,
132 caudally) and anterior auditory field (AAF, rostrally), a low-frequency reversal zone between
133 A1 and posterior auditory field (PAF, dorso-caudally), and a high-frequency reversal between

VAF and supra-rhinal auditory field (SRAF, ventrally). Thus, we could reliably define the lemniscal (A1, AAF, and VAF) and non-lemniscal (SRAF, PAF) auditory cortical fields as shown in Fig. 1b.

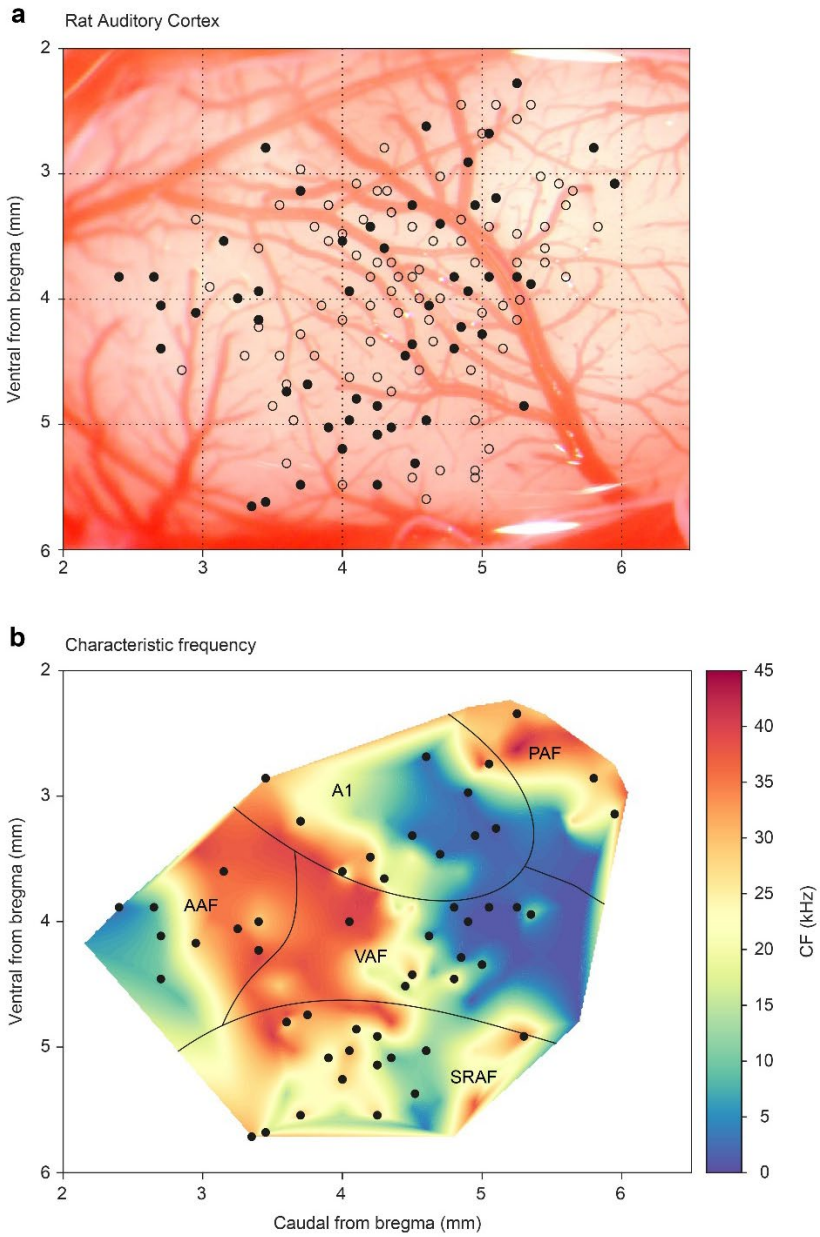

Figure 1: Map of all recording locations. *(a) All recording sites drawn over the cortex of a representative animal. At every site, the CF was determined and then we presented an oddball paradigm and the corresponding control sequences. (b) Distribution of the CFs across the entire rat auditory cortex. Note how each field shows a characteristic CF gradient. Empty dots indicate sites used only for CF determination. Filled dots indicate sites where oddball paradigm was recorded.*

146

147 **ACh modulates the magnitude of neuronal responses and nMM**

148 After the FRA was identified, we selected a pair of pure tones (10–30 dB above minimum
149 threshold) within the FRA at each recording site to test the adaptation of the neuronal
150 response under the oddball paradigm. To do so we quantified nMM using the common SSA
151 index (CSI). CSI values may range from -1 to +1, with negative values for units that respond
152 more to standard stimuli and positive values for units that respond more to deviant stimuli
153 (see Methods). In the following, we describe the effect of ACh on nMM (Figs. 2-6), in terms
154 of prediction error modulation and repetition suppression (Fig. 7). Figure 2 illustrates
155 representative responses of two units from the lemniscal auditory pathway — during and after
156 the injection of ACh — that showed a change in the CSI during ACh release (Fig. 2a and b,
157 decreased and increased CSI, respectively). Similarly, the non-lemniscal, divisions (high-
158 order regions) of the AC (Fig. 3) also show decreased and increased CSI during Ach
159 application (Figure 3a and b; respectively). In both Figure 2 and 3, peri-stimulus time
160 histograms (PSTH) are also depicted for standard- and deviant stimuli (blue and red lines,
161 respectively). On average, the firing rate decreased during the application of ACh (mean
162 control: 5.8 ± 7.0 spikes/s, mean ACh: 4.7 ± 10.3 spikes/s; Wilcoxon Signed Rank test, $p <$
163 0.001). Most neurons recovered their basal firing rates after 60-90 minutes after the ACh
164 injection (recovery mean: 6.5 ± 8.1 spikes/s, Wilcoxon Signed Rank test, $p = 0.4$, control vs.
165 recovery).

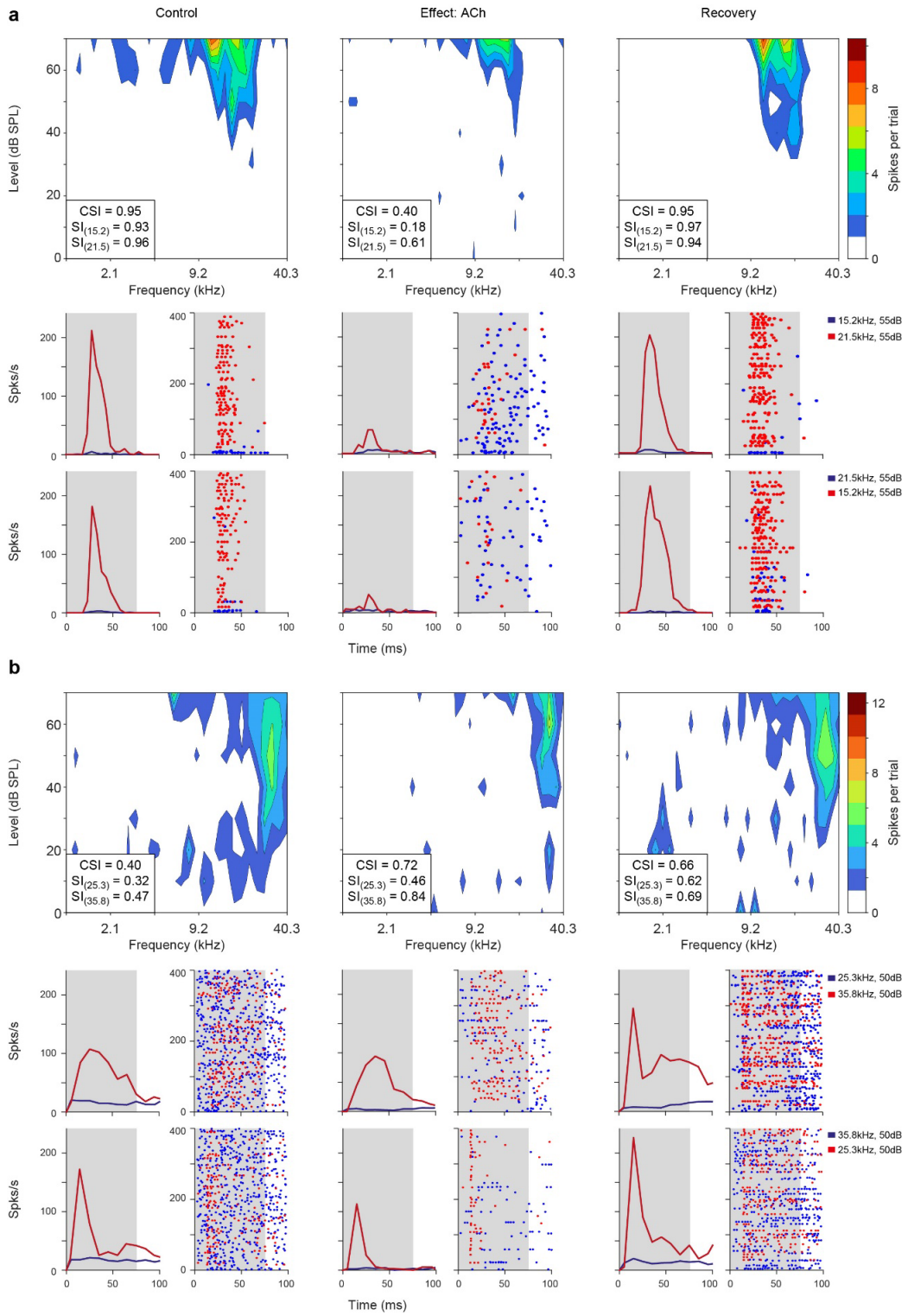

Figure 2: Examples of lemniscal AC units modulated by ACh. *Left, middle and right columns show the responses before (control), during (effect) and after (recovery) ACh application, respectively.* ***a.*** *FRAs and PSTHs from a unit located in A1. This specific neuron shows a CSI decrease during ACh application and recovery to baseline levels (CSI = 0.95, CSI= 0.4 and CSI = 0.95, respectively)* ***b.*** *FRAs and PSTHs from an AAF unit with increased CSI (CSI = 0.4, CSI= 0.72 and CSI = 0.66, respectively) during ACh application.*

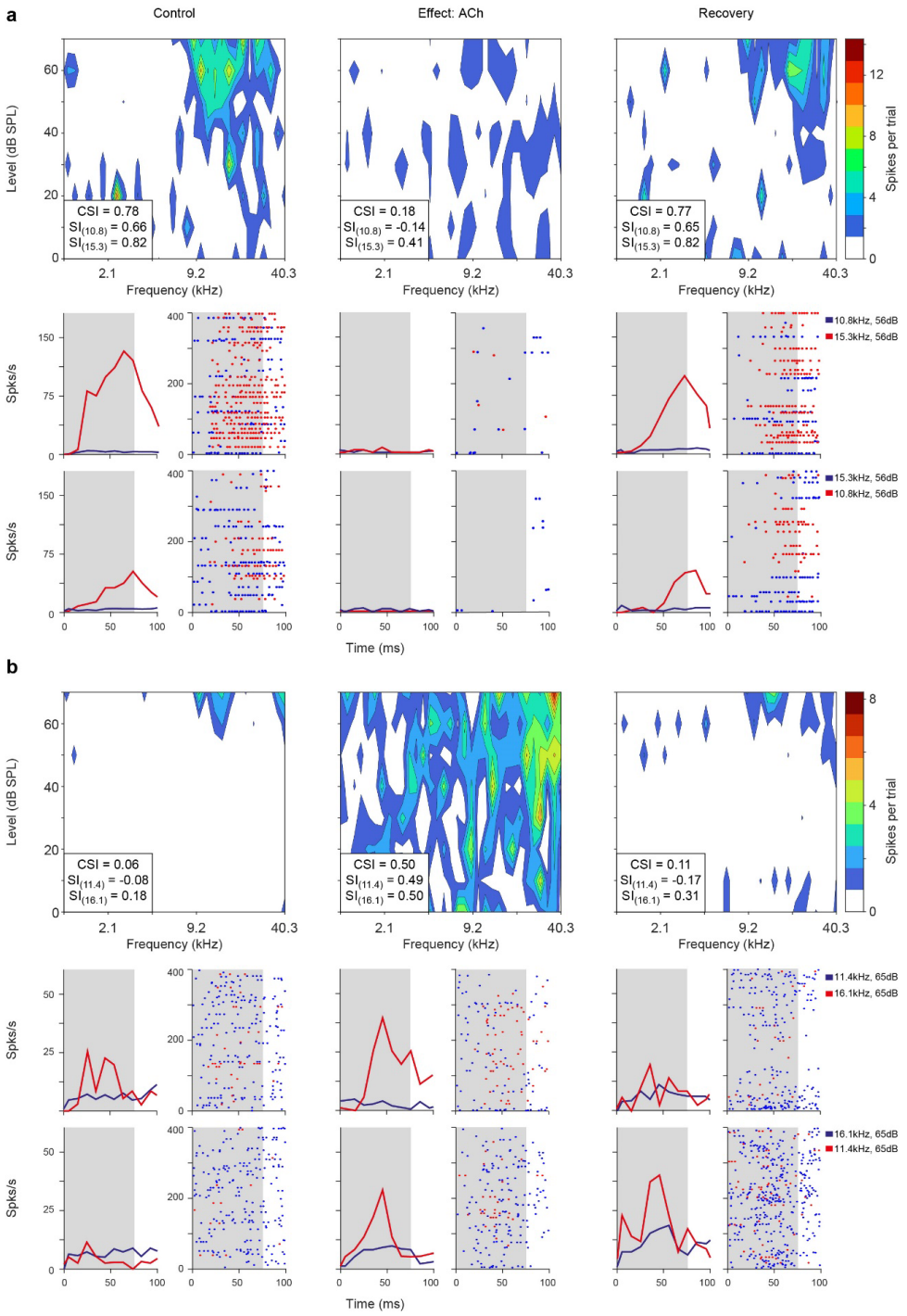

Figure 3: Non-lemniscal AC units modulated by ACh. *Left, middle and right columns show the responses before (control), during (effect) and after (recovery) ACh application, respectively.* ***a.*** *FRAs and PSTHs from a unit located in SRAF. This specific neuron shows a CSI decrease during ACh application and recovery to baseline levels (CSI = 0.78, CSI= 0.19 and CSI = 0.77, respectively).* ***b.*** *FRAs and PSTHs from a PAF unit with increased CSI (CSI = 0.06, CSI= 0.5 and CSI = 0.11, respectively) during ACh application.*

Given the changes in the FRAs observed in individual units during the application of ACh (Figs. 2 and 3), we checked for bandwidth changes at the population level. For that, we measured the FRA bandwidth in octaves at 10 and 30 dB above minimum threshold (BW10 and BW30, respectively). Numerous individual units showed either broadening or sharpening of their FRA bandwidth during ACh application, which were averaged out at the population level (Fig. 4a,b). Indeed, no significant changes occur in neither BW10 (control: 0.76±0.57 octaves; effect: 0.88±0.75 octaves; Wilcoxon signed rank test, p = 0.248) nor BW30 (control: 1.33±0.73 octaves; effect: 1.43±0.80 octaves; Wilcoxon signed rank test, p = 0.664) (Fig. 4c).

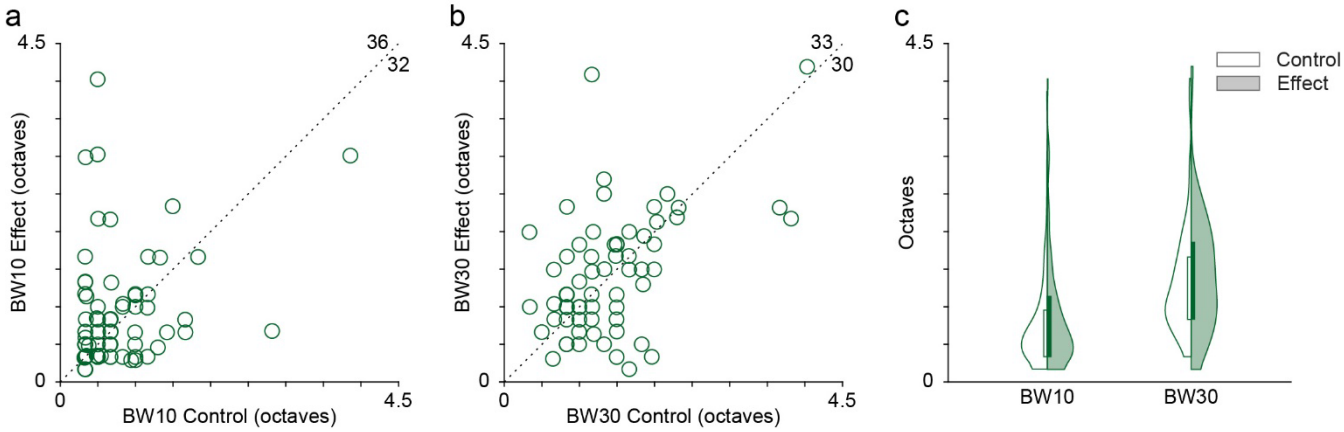

Figure 4: Effect of ACh on the bandwidth of the FRAs. *Many individual units showed enlarged or reduced FRA bandwidths, both at 10 (a) and 30 (b) dB above minimum threshold. The values in the upper-right corner of panels (a) and (b) indicate the number of units showing either an increment (top) or a decrement (right) of the bandwidth during the application of ACh. (c) Distribution of FRA bandwidths in octaves at 10 and 30 dB above minimum threshold (BW10 and BW30, respectively), before (white background) and during (shaded background) the application of ACh. ACh did not alter significantly neither BW10 nor BW30 at the population level.*

Next, we analyzed the effect of ACh on the CSI at the population level (n=85; comprising the neurons in our sample with significant responses to both F1 and F2 auditory stimuli). Figs. 2 and 3 illustrate four examples of units from lemniscal and non-lemniscal subdivisions before, during and after the application of ACh. Modulation of CSI levels was observed in all

individual examples. ACh produced a significant increase of the CSI value in 26 % (Fig. 5a, purple dots; 22/85, bootstrapping, 95% *c.i.*) and a significant decrease in 31% of the neurons recorded (Fig. 5a, orange dots; 26/85, bootstrapping, 95% *c.i.*). Thirty-seven units (43%) were unaffected by ACh. The average CSI during ACh injection (CSI = 0.54 ± 0.27) was similar to that of the control condition (CSI = 0.57 ± 0.23; Wilcoxon Signed Rank test, p=0.359; Fig. 5b).

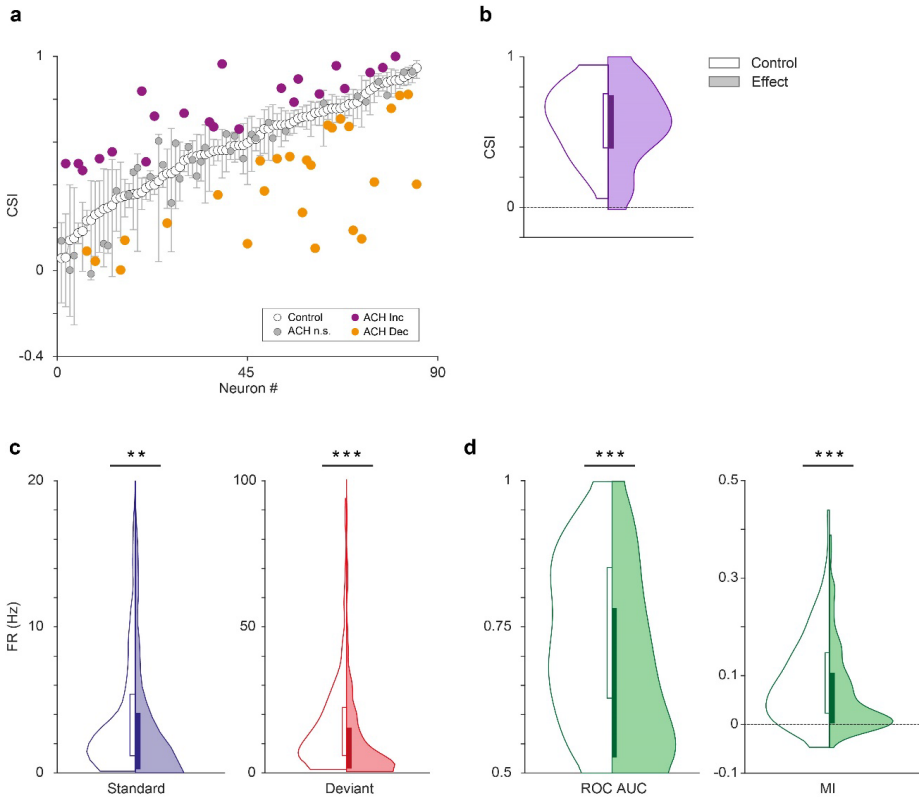

Figure 5: Effect of acetylcholine on CSI. *(a) Changes on the CSI due to the effect of ACh, for each recorded unit. The units are sorted based on their CSI in the control condition (white dots). The vertical bars indicate the 95% confidence interval for the CSI in the control condition. (b) Violin plots showing the CSI measured in control and effect conditions. The CSI did not change significantly during the application of ACH. In this and similar violin plots, white background indicates the control conditions, while shaded background indicates the effect condition. (c) Distribution of firing rates in response to the deviant (red) and standard tones (blue), in control and ACh conditions. The application of ACh caused a significant reduction in the response to both deviant and standard tones. (d) Distribution of AUC and Mutual Information values in control and ACh conditions. The application of ACh caused a significant decrease of both AC and Mutual Information. In this and similar figures: *p<0.05; **p<0.01; ***p<0.001.*

We analyzed the effect of ACh on the response to the deviant- or standard stimuli, separately. We observed that ACh produced a significant decrease in the mean firing rate in response to the deviant tones (Fig. 5c; 11.75 ±17.46 Hz), as compared to the control condition (16.51 ±16.19 Hz; Wilcoxon Signed Rank test, $p < 0.001$), as well as in the mean firing rate in response to standard tones (Fig. 5c; 4.58 ±6.38 vs 3.97 ±9.90 Hz, control vs ACh; Wilcoxon Signed Rank test, $p = 0.001$).

In order to establish how ACh affects discriminability of deviant- and standard stimuli — i.e. how well the stimulus identity can be decoded from the neuronal firing rate – we calculated the area under the curve (AUC) of the receiver operating characteristic (ROC) for each tone (Fig. 5d, left panel) and the Mutual Information to determine how much the response distributions for deviant- and standard stimuli overlap before and after ACh injections and how well the stimulus identity can be decoded from the neuronal firing rate. This is important because we can consider the response probability of the neuron, i.e., how many trials the neurons responded to. This analysis shows that the mean AUC decreased significantly during the application of ACh (0.74 ±0.13 vs 0.67 ±0.15, control vs. effect; Wilcoxon Signed Rank test, $p < 0.001$). The same happened for Mutual Information (Fig. 5d, right panel; 0.09 ±0.07 vs 0.07 ±0.08, control vs. effect; Wilcoxon Signed Rank test, $p = 0.003$). These AUC and Mutual Information analyses indicate that under the influence of ACh, neurons are less able to discriminate deviant stimuli from standard stimuli.

Different mechanisms for SI increase or decrease during ACh application

As mentioned above, the CSI is an indicator of the average level of nMM for a single unit, since it takes into account the responses of two frequencies (F1 and F2) that alternatively play the role of deviant and standard. However, in order to better understand the effect of ACh on

253 the response to each stimulus class — depending on whether it was presented as a deviant or
254 as a standard — the frequency-specific SSA index (SI, see Methods) is a better indicator. We
255 calculated the SI for 205 individual frequencies, from 113 units that elicited a significant
256 response to that particular frequency from our sample. This analysis shows that ACh
257 produced a significant increase of the SI in 27% of the frequencies recorded (Fig. 6a, purple
258 dots; 55/205, bootstrapping, 95% *c.i.*), 31% (64/205; Fig. 6a, orange dots) showed a
259 significant decrease of their SI and 42% frequencies (86/205) were unaffected by ACh. The
260 mean SI (SI = 0.55 ± 0.31, control condition) was reduced during ACh injection (SI = 0.40 ±
261 0.50) although this decrease was not significant (Wilcoxon Signed Rank test, p=0.086; Fig.
262 6b).

263 Since we found that the application of ACh had divergent effects on the SI (increase or
264 decrease), we further analyzed separately those two groups to identify different mechanisms.
265 We examined the firing rates in response to deviant- and standard stimuli, separately for those
266 frequencies showing a SI increase or decrease during the application of ACh. In both cases,
267 responses to the deviant- and standard stimuli were affected differently, when measuring the
268 firing rate change ratio (amount of change caused by ACh, relative to the baseline firing rate).
269 In frequencies showing SI increase, the effect of ACh was significantly different for the
270 deviant- and standard stimuli (Fig. 6c, top panel; p<0.001, Wilcoxon signed rank test).
271 Furthermore, this ratio was clearly negative for deviant sounds (p<0.001, Wilcoxon signed
272 rank test) and not significant for standards (p=0.256, Wilcoxon signed rank test), indicating
273 that ACh caused a reduction of the firing rate differentially during deviant stimuli. On the
274 other hand, in frequencies showing SI increase the effect of ACh also had a distinct effect on
275 the deviant- and standard stimuli (Fig. 6d, top panel; p<0.001, Wilcoxon signed rank test), but
276 in this case the effects were reverse: the change ratio was clearly negative for standard sounds
277 (p=0.001, Wilcoxon signed rank test) and not significant for deviant ones (p=0.379, Wilcoxon

signed rank test), hence ACh caused a reduction of the firing rate solely during standard stimuli. In other words, while the effect of ACh was a reduction of the firing rate, in some frequencies it only affected responses to the deviant stimuli, thus decreasing SI (Fig 6c, top panel), while in others it only affected responses to the standard stimuli, resulting in an increment of the SI (Fig 6d, top panel).

Interestingly, stimuli discriminability was affected differently by ACh in both groups. In frequencies showing SI decrease (Fig. 6c, bottom panel) both ROC AUC and Mutual Information decreased significantly during ACh application ($p<0.001$in both cases, Wilcoxon signed rank test), in line with the results obtained for the whole sample (compare to Fig. 5d). However, in frequencies showing SI increase (Fig. 6d, bottom panel) ROC AUC did not change significantly ($p= 0.339$), while Mutual Information increased slightly ($p= 0.008$). These results suggest that frequencies showing SI decrease are the ones mediating the main effects of ACh in the population.

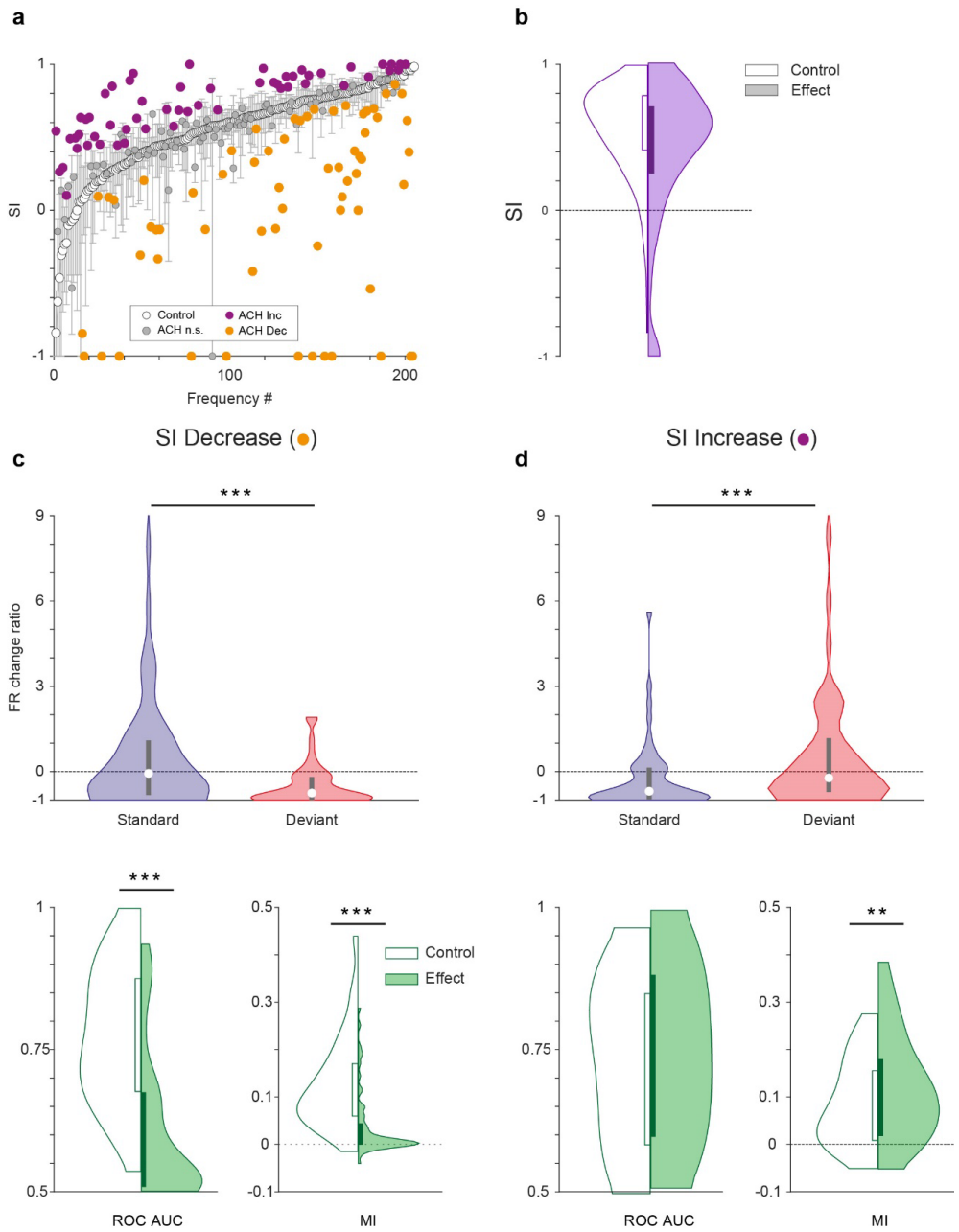

Figure 6: Characteristics of units depending on the effect of ACh on SI. *(a) Changes on the SI due to the effect of ACh, for each tested tone. The units are sorted based on their SI in the control condition (white dots). The vertical bars indicate the 95% confidence interval for the SI in the control condition. (b) Violin plot depicting the overall effect of ACh on the SI, for the complete sample. (c) Firing rate change ratio due to ACh application, relative to the control condition. In units showing SI decrease (left column), it was caused by a significant reduction of the firing rate in response to deviant tones. By contrast, in units showing SI increase (right column) it was caused by a significant reduction of the firing rate in response to standard tones. (d) In units showing SI decrease (left column) there was a significant reduction of both AUC and Mutual Information during the application of ACh. On the other hand, in units showing SI increase (right column) AUC did not change but Mutual Information increased.*

306

307 **ACh affects neuronal mismatch, modulating prediction error responses but not**
308 **repetition suppression**

309 According to the predictive coding framework, nMM can be split in two functionally distinct
310 components: prediction error modulation (i.e., an increased response to an oddball caused by
311 the violation of a regularity) and repetition suppression (i.e., reduction in the response to a
312 standard caused by sensory learning of a repeated stimulus). These differential effects can be
313 quantified by comparing the responses to the oddball paradigm with a suitable control
314 sequence (Fig. S1). Therefore, to test if ACh modulates prediction error signaling in AC, we
315 also recorded the cascade control sequence (for the corresponding oddball sequences) in 66
316 neurons of the sample, using an approach previously published (Carbajal and Malmierca,
317 2018; Parras et al., 2017; Ruhnau et al., 2012; Valdés-Baizabal et al., 2019). First, we
318 calculated the normalized spike counts in response to the cascade control, deviant and
319 standard stimuli (CAS, DEV and STD, respectively; see Methods). ACh led to a significant
320 decrease in the DEV responses in those units where SI decreased (Fig 7a; Wilcoxon Signed
321 Rank test, $p<0.001$) and to a significant increase in those units were SI increased (Fig 7b; $p=$
322 0.011). The opposite effect occurs on STD stimuli, increasing in units where SI decreased
323 (Fig 7a; $p<0.001$) and decreasing in units where SI increased (Fig 7b; $p<0.001$). While this
324 trend is very clear, there were no significant changes in CAS ($p=0.091$ and $p = 0.072$, for SI
325 decrease and increase, respectively).

326

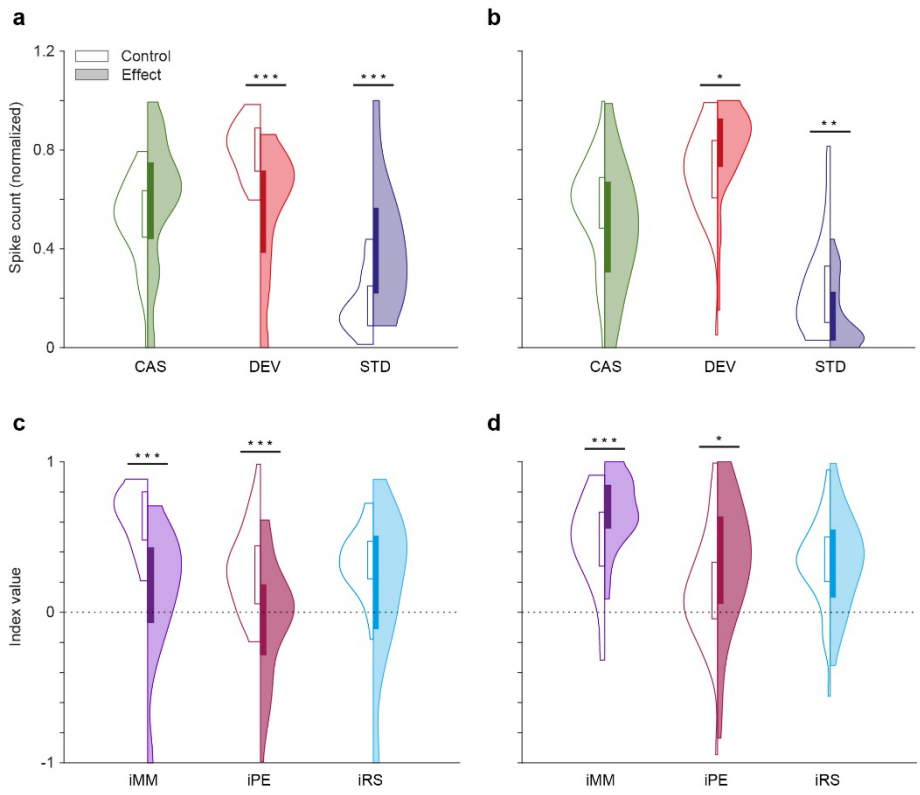

Figure 7: Predictive coding indices depending on the effect of ACh on SI. *The application of ACh decreased the normalized spike counts in response to deviant stimuli (red) and increased the normalized spike counts in response to standard stimuli (blue) in those units where SI decreased due to the application of ACh (a), while the changes were opposite in those units where SI increased due to the application of ACh (b). In neither case, did the response to the cascade condition (green) change significantly, but there was a slight trend in the same direction as the changes of the standards. In consequence, the neuronal mismatch (iMM, purple) and prediction error indexes (iPE, light red) decreased significantly in those units where SI decreased due to the application of ACh (c), but increased in those units where SI increased due to the application of ACh (d). The repetition suppression index (iRS) in light blue, did not change significantly in any case.*

Using the normalized CAS, DEV and STD responses, we computed the indexes iMM, iPE and iRS before and after the ACh injection in SI decrease units (Figure 7c, iMM: 0.63 ± 0.19 vs 0.13 ± 42; iPE: 0.29 ± 0.27 vs -0.05 ± 0.38; iRS: 0.34 ± 0.20 vs 0.17 ± 0.49; control vs ACh, respectively) and SI increase units (Figure 7d, iMM: 0.47 ± 0.31 vs 0.67 ± 0.22; iPE: 0.15 ± 0.36 vs 0.33 ± 43; iRS: 0.32 ± 0.30 vs 0.34 ± 0.31). iMM is equivalent to the CSI, but

348 using normalized response values, and since it includes information about the cascade control,
349 it can be divided into prediction error and repetition suppression components (iPE and iRS,
350 respectively; see Methods and Fig. S1c). Significant effects of ACh administration were
351 found for iMM and iPE, both in SI decrease units (iPE: $p<0.001$; iMM: $p<0.001$; Wilcoxon
352 Signed Rank test; Fig. 7c) and SI increase units (iPE: $p = 0.023$; iMM: $p<0.001$; Wilcoxon
353 Signed Rank test; Fig. 7d), while iRS remained unchanged (SI decrease units iRS: $p = 0.121$;
354 SI increase units iRS: $p = 0.675$; Wilcoxon Signed Rank test).

355

356 Under the predictive coding framework, the precision of prediction errors encodes the
357 confidence or reliability afforded such errors (Friston, 2008), enabling precise prediction
358 errors to access higher levels of the auditory hierarchy. To test whether neuronal responses
359 show differential effects of precision weighting — depending on their level of deviance
360 sensitivity – we split our sample in two similar-sized groups (of frequencies), using the
361 median SI as cutoff (0.6143: SI before the application of ACh): low SI (n = 65 frequencies
362 with cascade control) and high SI (n = 66 frequencies with cascade control) (Fig. 8a-c). Given
363 this grouping, we found that ACh decreased significantly iMM (0.72±0.13 vs 0.52±0.36,
364 control vs effect; $p<0.001$) and iPE (0.33±0.33 vs 0.145±0.48, control vs effect; $p=0.004$) in
365 high SI frequencies, while only decreasing iRS significantly in low SI frequencies (0.28±0.25
366 vs 0.18±0.36, control vs effect; $p<0.037$) (Fig. 8a-c, top row).

367 Given the divergent defects of ACh on putative prediction error modulation we hypothesized
368 that acetylcholine would increase the variance of deviance-sensitive responses over groups of
369 cells. We calculated the variance of the above distributions of predictive coding indexes
370 (iMM, iPE and iRS) as an estimate of the (inverse of) their precision, as well as its 95%
371 confidence interval using a 1000-sample bootstrap strategy, and then used an F-test to check
372 for differences in the variances before and during ACh application (Fig. 8a-c, bottom row).

These results demonstrate that ACh application significantly increases the variance of iMM and iRS for both low SI and high SI groups, but interestingly Ach also significantly increase the variance of iPE only for the high SI group.

Then, we repeated the same variance analysis grouping the frequencies based on the anatomical layer location (depth) of the recording sites (Fig. 8d-f). In this case we split the frequencies into deep and superficial, with a depth cutoff of 650 µm, which is near the boundary between layers IV and V in the rat AC (Games and Winer, 1988; Malmierca, 2015). In this case, we found no significant effect of ACh on iMM, iPE nor iRS for none of the depth groups (Fig. 8d-f, top row). However, the general trend was an increase in the variance for all indexes and depth groups during the application of ACh (except for iPE in superficial units), which was significant for all indexes in the case deep units only (Fig. 8d-f, top row).

Thus, our results indicate that ACh produces a general increase of the variance for iMM, iPE and iRS. This general increase occurs regardless of the baseline SI value, but is more noticeable for neurons located in the infragranular layers.

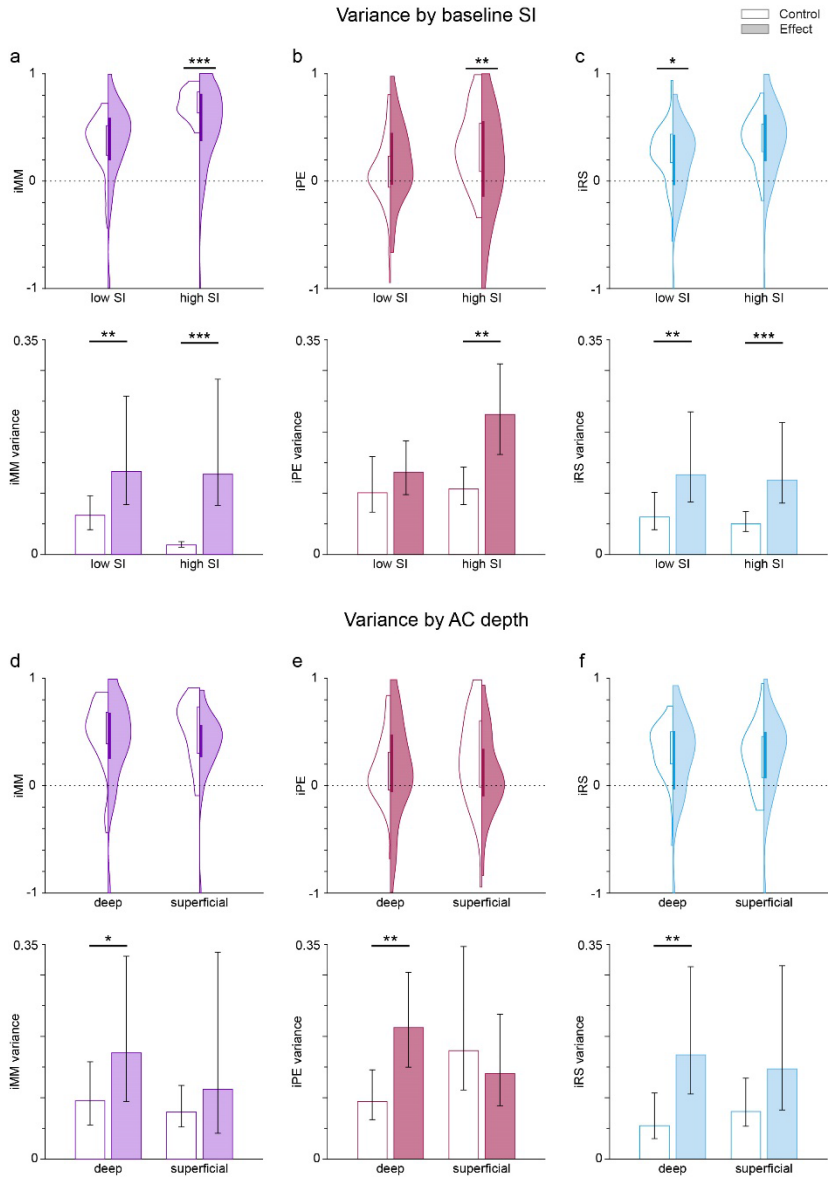

387

388 ***Figure 8: Dependence of the variance of predictive coding indexes on the SI before ACh***
389 ***application, as well as and on AC depth***. *Violin plots show the distribution of the iMM, iPE*
390 *and iRS indexes based on the SI value before application (a-c; low SI: SI < 0.6143; high SI:*
391 *SI < 0.6143, see text) or the AC depth (d-f; deep: >650 µm; superficial: <650 µm). Bar*
392 *graphs show the variance of the related indexes. Error bars indicate 95% CI. The results*
393 *before ACh application are shown in a white background (control), while shaded*
394 *backgrounds represent the results during ACh application (effect). The application of ACh*
395 *reduced significantly iMM and iPE (a and b, top row) for those frequencies with high*
396 *baseline SI, as well as iRS (c, top row) for frequencies with low baseline SI. The variance of*
397 *all indexes increased significantly during ACh application, except for the iPE of the low SI*
398 *group. Regarding the depth of the recording sites, ACh did not significantly change the*
399 *values of any indexes, neither for deep nor for superficial units (d-f, top row). However, ACh*
400 *significantly increased the variance of all indexes for deep units, but not for superficial units*
401 *(d-f, bottom row).*

402

403

404 **ACh effect on nMM as a function of topographic distribution**

405 A remaining question is whether the effect of ACh is uniformly distributed across AC neurons
406 in different fields and layers. Figure 9 shows the CSI (first row) and spike count levels for the
407 standard and deviant tones (middle and bottom rows, respectively) before and after ACh
408 application, as well as the difference between the ACh and control conditions. The highest
409 levels of CSI in the control condition (left column) were found in SRAF. ACh application
410 (middle column) produced an overall increment of CSI in AAF and a decrement in the rest of
411 the fields, however such changes did not reach statistical significance ($p>0.79$ in all fields,
412 Wilcoxon signed rank test with Holm-Bonferroni correction). Regarding the responses to the
413 standard stimuli (middle row), ACh application caused an increase of the firing rate in A1 and
414 PAF, and a decrease in AAF, VAF and SRAF, but such changes were only significant in AAF
415 ($p=0.001$, Wilcoxon signed rank test with Holm-Bonferroni correction). By contrast, the
416 firing rates in response to the deviant sounds (bottom row) decreased in all fields during ACh
417 application, with significant changes in AAF, VAF and SRAF ($p=0.011$, $p=0.026$ and
418 $p=0.009$, respectively; Wilcoxon signed rank test with Holm-Bonferroni correction).

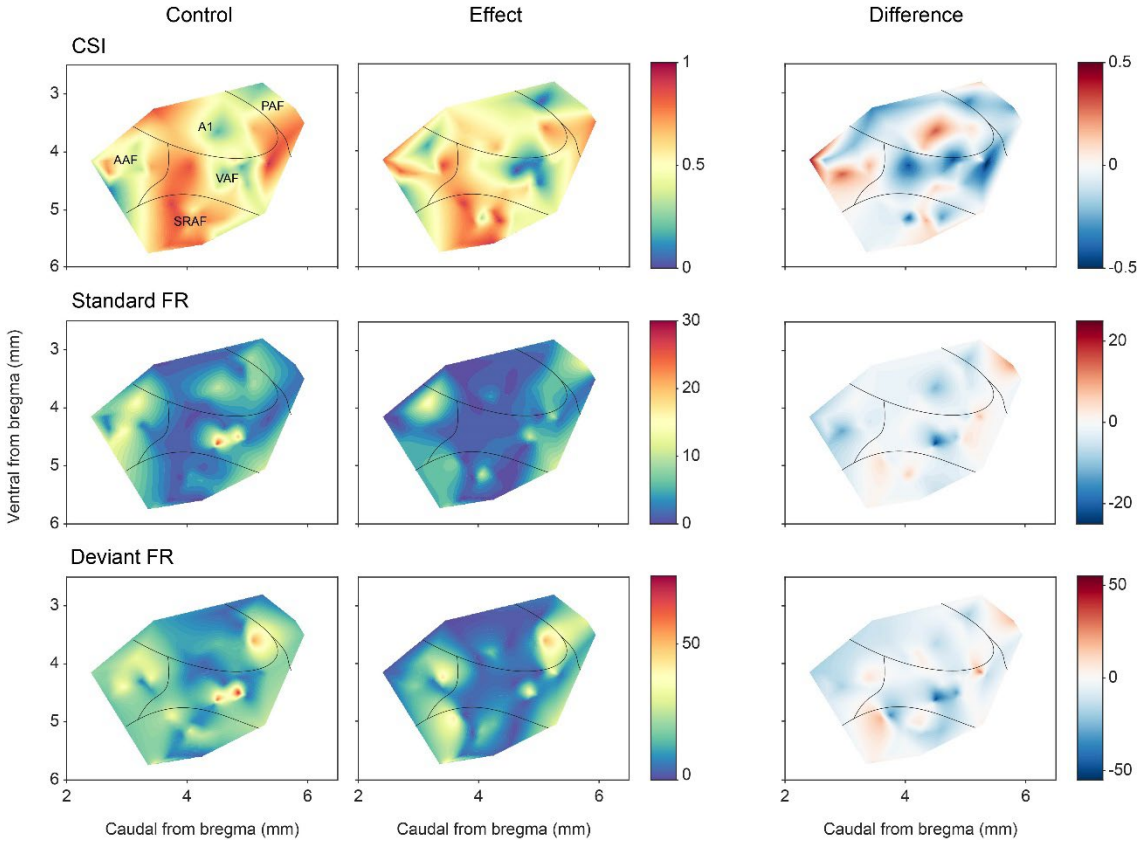

Figure 9: Anatomical localization of CSI and responses to the deviant and standard tones. *Distribution of CSI (top row) and responses (spikes per trial) for deviant (bottom row) and standard tones (middle row), before and after ACh application, as well as the difference between both conditions.*

In order to better understand the effect of ACh on the responses to the individual frequencies of the oddball paradigm (F1 and F2), we calculated the SSA index (SI) independently for each of the paradigm frequencies. We found that ACh was more likely to cause a SI decrease in all AC fields except for AAF, where ACh was more likely to cause an SI increase (Fig. 10a). Figure 10b shows the distribution of recording depths within the AC, for those units that showed a significant SI decrease (orange) or increase (purple) during the application of ACh. The shaded background shows the probability density function for those distributions. We found that frequencies that experienced an SI decrease during ACh application were most likely located in the granular layer (layer IV) or the upper infragranular regions (dorsal parts

of layer V). In contrast, frequencies that experienced an SI decrease during ACh application were more likely located in deeper infragranular regions (layers V and VI).

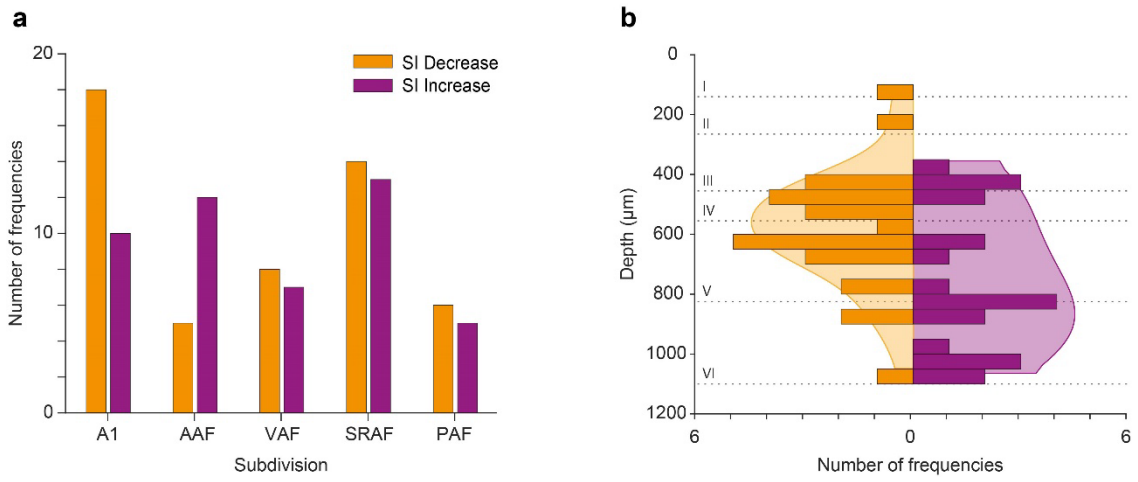

Figure 10: Effect of ACh on* nMM *in AC fields and layers. *(a) Number of tested frequencies in which SI decreased (orange) or increased (purple) for each AC field. In A1 it is more likely to find frequencies showing SI decrease, while in AAF it is more likely to find those showing SI increase. In VAR, SRAF and PAF, the likelihood of both types is similar. (b) Distribution of tested frequencies in which SI decreased (orange) or increased (purple) significantly due to the effect of ACh, across AC layers. The shaded background depicts the probability density functions. Note that units experiencing SI decrease are more prevalent around the granular layer (layer IV), while units experiencing SI increase are more commonly found in the infragranular layers.*

DISCUSSION

We recorded neuronal responses from the AC under an auditory oddball paradigm while performing microiontophoretic applications of ACh to investigate the role of the cholinergic system in the processing of unexpected or surprising events. Furthermore, we employed cascade sequences to control for repetition suppression and assess cholinergic effects on prediction error relative to repetition suppression. Our results show that 1) ACh modulates nMM, evidenced as decrements or increments of the neuronal mismatch indexes (iMM, iPE and iRS). The decreased SI is due to a diminished response to the deviant tone while increased SI is the consequence of a

diminished response to the standard sounds (Fig. 6, and examples in Figs. 2-3); 2) ACh exerts a global and distributed effect on AC neurons that is layer specific but field unspecific (Figs. 9,10); 3) The decreased- and increased SI are driven by the effects of ACh on iPE but not iRS (Fig. 7), and 4) ACh increases the variance of iMM, iPE and iRS. Together, these findings reveal how ACh modulates prediction error signals and repetition suppression differentially in the AC, likely gating these signals, as they ascend beyond the auditory cortex to frontal, higher cognitive regions.

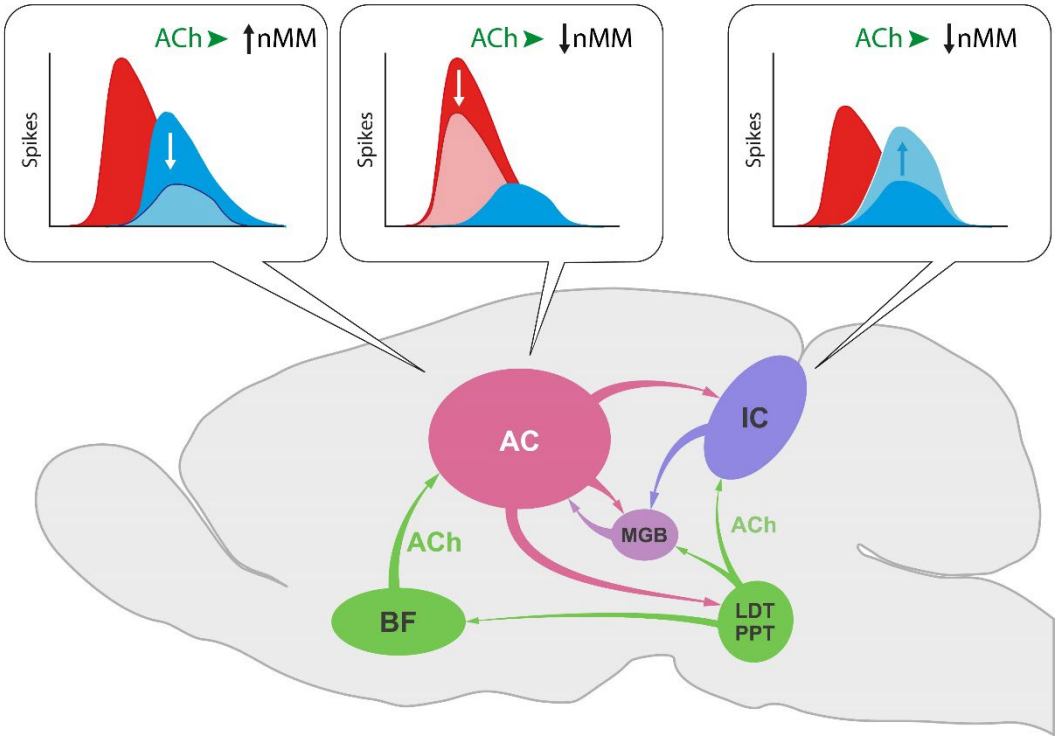

Figure 11: Effect of ACh on nMM in auditory midbrain and cortex. *ACh increases nMM in the AC reducing the firing rate in response to either 'deviants' or 'standards', while it shows a different effect in the IC, as ACh decreases nMM by increasing the responses to the 'standard' tones (Ayala and Malmierca, 2015). These divergent effects may be explained by the different connectivity of both auditory areas. While the AC receives its cholinergic input from the basal forebrain (BF), the IC is innervated by the pedunculopontine (PPT) and laterodorsal tegmental (LDT) regions in the brainstem. This intersection of auditory and cholinergic nuclei creates an intricate network involving ascending and descending projections that ultimately modulate the processing of auditory deviance detection.*

478 ACh increases the amplitude of AC neuronal responses to sound stimulation, decreases the
479 auditory threshold and sharpen the receptive field in the AC. (Edeline, 2012; Irvine, 2018a,
480 2018b; Kilgard and Merzenich, 1998; Ma and Suga, 2005; Metherate, 2011; Metherate et al.,
481 1992; Puckett et al., 2007). These ACh-mediated effects are produced by a rapid disinhibition
482 of neuronal responses, modifying synaptic strength, enhancing excitatory-inhibitory balance
483 and reorganizing cortical circuits promoting cortical plasticity (Froemke et al., 2007; Irvine,
484 2018a, 2018b; Metherate, 2011; Picciotto et al., 2012). But ACh also produces direct
485 inhibitory effects leading to a decrease of cortical responses (Colangelo et al., 2019; Dasgupta
486 et al., 2018; Eggermann and Feldmeyer, 2009; Qi and Feldmeyer, 2022). Our results confirm
487 these mixed effects (excitatory and inhibitory, during the application of ACh) at the neuronal
488 level. However, when looking at the population level, the overall effect in our sample was a
489 differential reduction of the responses to either deviant or standard stimuli. Apart from the
490 direct hyperpolarizing effect of ACh on some cell types, it is also possible that some of the
491 recorded neurons received direct inhibitory inputs, and those inhibitory neurons were the ones
492 affected by ACh. By increasing the firing rates of such inhibitory interneurons, the observed
493 overall effect of ACh could lead to a reduction of the activity on the recorded neurons. An
494 important functional motif — for state modulation in the cortex — is through disinhibition
495 consisting of parvalbumin-, somatostatin-, and vasoactive intestinal peptide- expressing
496 interneurons. When the latter receive cholinergic projections from the basal forebrain , they
497 remove the inhibition on layer 2/3 pyramidal neurons exerted by somatostatin interneurons (Fu et
498 al., 2014). The connectivity relationships among inhibitory neurons seems to be critical.
499 Moreover, it has been recently described how each of those cell types respond differently to
500 deviants and standards in the auditory cortex (Yarden et al., 2022).

501 ACh plays important roles in arousal, attention, and sensory learning (Hasselmo, 1999;
502 Hasselmo and Sarter, 2011; Metherate, 2011; Picciotto et al., 2012; Sarter et al., 2001;

503 Weinberger, 2004). Thus, it is not surprising that ACh may have a critical role in shaping
504 nMM, which has many properties in common with behavioral habituation to a repeated
505 stimulus and can be considered a simple form of learning (Irvine, 2018a; Nelken, 2014;
506 Netser et al., 2011). Furthermore, a recent study in rats has shown that the administration of
507 muscarinic ACh receptor agonists and antagonists affected MMN amplitude in A1 and PAF
508 (Schöbi et al., 2021), suggesting that the cholinergic system modulates the connectivity
509 between those areas during the occurrence of deviant sounds. But to the best of our
510 knowledge, the present study demonstrates a specific effect of ACh on prediction error
511 responses.

512 In the IC, ACh selectively increased the response to the repetitious standard stimulus (Ayala
513 and Malmierca, 2015), while we show here that ACh in the AC not only increases the
514 responses to the unexpected deviant sounds leading to an increase of SI (Fig. 6d) but also
515 decreases responses to the repeated standard that result in a diminished CSI index (Fig. 6c).
516 This divergent effect of ACh on subcortical and cortical nMM may be related to the different
517 origin of ACh and/or the unique organization of neuronal circuitries in IC and AC (Fig. 11).
518 While the sources of ACh to IC emerge from the pedunculopontine and laterodorsal tegmental
519 regions in the brainstem (Motts and Schofield, 2009), those to AC originate in the basal
520 forebrain (Chavez and Zaborszky, 2017).

521 According to the predictive coding formulations, cortical areas send predictions to lower
522 hierarchical areas to inhibit neuronal populations encoding prediction errors. When top-down
523 predictions match bottom-up sensory input, the prediction error response is attenuated.
524 Conversely, those lower areas send error information to higher hierarchical centers when
525 event predictions fail to drive higher level representations and improve the top-down
526 predictions. If a stimulus is not predicted, the difference between predicted and received
527 inputs yields large prediction errors, while if a stimulus is constantly repeated, sensory

learning enables more accurate predictions and a decrease in prediction error responses – a phenomenon referred to as repetition suppression (Auksztulewicz and Friston, 2016). Thus, nMM can be explained under the predictive coding framework (Carbajal and Malmierca, 2018; Parras et al., 2017), and recent studies that found LFP and spiking responses to omitted tones in the rat auditory cortex (Auksztulewicz et al., 2023; Lao-Rodríguez et al., 2023), among others, strongly support this interpretation. However, predictions and prediction errors may also be modulated in a context-dependent manner, meaning that responses can be modulated and given precedence depending on the context in which the stimulus is perceived (Keller and Mrsic-Flogel, 2018). The source of such a modulating or gating signal may arise from neuromodulatory inputs (Fu et al., 2014; Moran et al., 2013; Pinto et al., 2013; Polack et al., 2013; Thiele and Bellgrove, 2018) that can not only gate plasticity (Kilgard and Merzenich, 1998; Martins and Froemke, 2015; Weinberger, 2004), but also change the balance of top-down versus bottom-up influence (Yu and Dayan, 2002).

Within the predictive coding framework, classical neuromodulators such as ACh are often thought to increase the precision of prediction error signaling (Auksztulewicz et al., 2018; Auksztulewicz and Friston, 2016; Feldman and Friston, 2010; Moran et al., 2013). Indeed, Yu and Dayan (Yu and Dayan, 2005, 2002) proposed that ACh levels reflect the "expected uncertainty" (when there is less confidence in the prediction) associated with top-down information and modulate the interaction between top-down and bottom-up processing in determining the appropriate neural representations for inputs (Auksztulewicz et al., 2017; Yu and Dayan, 2005, 2002). Thus, the precision of prediction errors would encode the confidence or reliability afforded of such errors (Friston, 2005), increasing the influence of precise prediction errors on higher-level processing. Thus, the canonical view – within the predictive coding framework — is that precision would affect postsynaptic gain through the action of neuromodulators such as ACh, enhancing the responses of units broadcasting prediction

errors. Using computational neuronal modeling and EEG recordings under oddball paradigms in subjects manipulated pharmacologically with galantamine (a competitive inhibitor of acetylcholinesterase, Moran et al. (2013) have shown that ACh enhances the precision of bottom-up synaptic transmission in cortical hierarchies by optimizing the gain of supragranular pyramidal neurons, amounting to an increase in the precision of prediction error signaling. Thus, our results and those from Moran and colleagues (2013) suggest that ACh mediates the representation of precision.

Our results are consistent with this predictive coding picture; particularly when noting that and increase in precision leads to a representational sharpening (Kok et al., 2012a), in which the majority of (prediction error) neurons are suppressed and a few neurons encoding precise prediction errors are enhanced (Friston, 2018; Kok et al., 2012a; Shipp, 2016). This is consistent with the effect of acetylcholine on average over neurons studied and the differential effect on standard and oddball responses; dependent upon their SI.

ACh increases the variance the prediction error component of neuronal responses in those units with higher SI (Fig. 8b, top), especially in units with strong deviance detection properties (Fig. 8b, bottom). This finding suggests that ACh plays the key role in encoding of precision or uncertainty. Interestingly, ACh not only increases the variance of prediction error responses, but also the variance of repetition suppression (Fig. 8c).

A change in the precision of prediction errors may denote — or alert to — a variable environment, where it is difficult to extract rules and only generate weak (and less useful) predictions. Under this scenario, some fluctuations in the sensory input can be expected, assigning less precision to prediction errors (Yon and Frith, 2021). If so, ACh would adjust the predictions' confidence, so we would not be surprised by small changes in the environment, since they are likely, expected noisy, fluctuations. Otherwise, an excessive

577 confidence on predictions in a volatile environment may override the incoming evidence,
578 leading to the false inference of expected by absent events (Yon and Frith, 2021).

579 Attention is thought to boost the precision of prediction errors (Kok et al., 2012b), and our
580 experiments carried out under anesthesia clearly lack attention, where baseline cholinergic
581 activity is low, making it difficult to interpret how the results generalize to more ecologically
582 valid situations (Minces et al., 2017). Interestingly, there is a wealth of data suggesting that
583 minimal impairments to the encoding or defective signaling of precision or uncertainty are
584 sufficient to explain psychopathic conditions impaired such as schizophrenia or autism
585 (Friston, 2023). Furthermore, it is unclear to what degree the amount of agonist liberated
586 used iontophoretic application of cholinergic agonists emulates a relevant physiological
587 condition (Minces et al., 2017). Future studies using optogenetic techniques to activate only
588 basal forebrain cholinergic neurons while also recording from auditory cortex neurons, will
589 allow a fine-grained investigation of the role of cortical acetylcholine on sensory
590 representation. Moreover, using an awake preparation will confirm a definitive corroboration
591 of the effect of ACh on precision. The available neurobiological evidence suggests that
592 precision is encoded by the synaptic gain of superficial pyramidal cells encoding prediction
593 errors, which are controlled by neuromodulatory systems (e.g., dopaminergic, cholinergic)
594 and/or synchronized neural activity (Feldman and Friston, 2010; Kok et al., 2012b). However,
595 we do not find changes in prediction error precision in the superficial layers; our analysis
596 suggests instead that the effects of ACh were more limited to the deep AC layers (Fig. 8e).
597 We observed a distinct and differential distribution of units throughout the cortical layers,
598 contingent upon the influence of ACh on their selectivity index (SI). Units exhibiting an SI
599 decrease during ACh application were predominantly located and biased in layers III-IV and
600 its adjacent regions, while those demonstrating an SI increment during ACh application
601 spanned from the deeper layer IV to layer VI (Fig. 10b).

602 In the initial conceptualizations of predictive coding, it was posited that prediction units reside
603 in the infragranular layers (layers V and VI), with error units situated in supragranular layers
604 (layers I – III) (Bastos et al., 2012; Friston, 2005). Alternatively, some models suggest that
605 error units would be localized in the granular layer (layer IV), while prediction units would be
606 detected in both supra- and infragranular layers (biased competition model of predictive
607 coding; Spratling, 2008). In our recordings, units displaying an SI reduction during ACh
608 application were also those with a higher SI under baseline conditions (i.e., larger response to
609 deviant than to standard stimuli), thereby potentially qualifying as error units. These units
610 were identified in layer IV and neighboring areas, which appears to support the model
611 proposed by Spratling (2008). Furthermore, according to Eggermann and Feldmeyer (2009),
612 the application of ACh would filter weak sensory inputs to layer IV and amplify signals at
613 superficial and deep layers, effectively increasing the signal to noise ratio. In contrast, units
614 demonstrating an SI increase during ACh application could be considered potential prediction
615 units; such units were detected in granular and deep layers but were absent in superficial
616 layers. This observation aligns with both predictive coding models, as each postulate that deep
617 layers contain prediction units.

618 In conclusion, we have shown that ACh plays a multifold role in modulating nMM in
619 AC, affecting the precision of prediction error signaling and gating prediction errors to
620 hierarchically higher processing levels.

621

622 **MATERIALS AND METHODS**

623 **Subjects and surgical procedures**

624 The experimental protocols were approved conforming to the University of Salamanca
625 Animal Care Committee standards and the European Union (Directive 2010/63/EU) for the

use of animals in neuroscience research. Experiments were performed on 37 adult female Long-Evans rats with body weights within 180-250 g. Surgical anesthesia was induced and maintained with urethane (1.5 g/kg, intraperitoneal), with supplementary doses (0.5 g/kg, intraperitoneal) given as needed. Dexamethasone (0.25 mg/kg) and atropine sulfate (0.1 mg/kg) were administered at the beginning of the surgery to reduce brain edema and the viscosity of bronchial secretions, respectively. Normal hearing was verified with auditory brainstem responses (ABR) recorded with subcutaneous needle electrodes, using a RZ6 Multi I/O Processor (Tucker-Davis Technologies, TDT) and processed with BioSig software (TDT). ABR stimuli consisted of 100 µs clicks at a 21/s rate, delivered monaurally to the right ear in 10 dB steps, from 10 to 90 decibels of sound pressure level (dB SPL), using a closed-field speaker. After the animal reached a surgical plane of anesthesia, the trachea was cannulated for artificial ventilation and a cisternal drain was introduced to prevent brain hernia and bran edema. Isotonic glucosaline solution was administered periodically (5–10 ml every 7 h, subcutaneous) throughout the experiment to prevent dehydration. Body temperature was monitored with a rectal probe thermometer and maintained between 37 and 38°C with a homoeothermic blanket system.

The auditory cortex surgery was described in previous works (Nieto-Diego and Malmierca, 2016; Parras et al., 2017) . The temporal bone was exposed and the auditory cortex was located using stereotactic coordinates (Paxinos et al., 1997). A craniotomy was performed over the auditory cortex, the dura was removed carefully, and the exposed area was filled with a layer of agar to prevent desiccation and to stabilize the recordings. Before applying the agar, a magnified picture (25×) of the exposed cortex was taken with a digital camera coupled to the surgical microscope (Zeiss) through a lens adapter (TTI Medical). The picture included a pair of reference points previously marked on the dorsal ridge of the temporal bone, indicating the absolute scale and position of the image with respect to bregma (the reference point). This

picture was displayed on a computer screen and was overlapped with a micrometric grid, over which the placement of the multibarrel for every recording was marked. The micrometric grid allowed to generate coordinates in a two-dimensional axis, from the superimposed image of the auditory cortex of each animal. Once the coordinates of each of the recorded units of all the animals were obtained, we used the functions 'griddata' and 'contourf' of MATLAB to generate topographic maps (through a graduation of colors) of the characteristic frequency (CF), Common SSA Index (CSI) levels, and deviant and standard tone responses in all auditory cortical fields.

Electrophysiological recording and microiontophoresis

A tungsten electrode (1–3 MΩ) was used to record multiunit neuronal activity. It was attached to a 5-barrel multibarrel borosilicate glass pipette that carried drug solution to be delivered in the vicinity of the recorded neuron. The multibarrel's tip was cut to a diameter of about 20-30 µm approximately. The center barrel was filled with saline solution for current compensation (165 mM NaCl) whereas the others barrels were filled with 1 M acetylcholine chloride (Sigma, catalog no. A6625). The pH was adjusted between 4.0-4.2 (Ayala and Malmierca, 2015). Drugs were retained by applying a -15 nA current, and were ejected when required, typically using 30–40 nA currents (Neurophore BH-2 System, Harvard Apparatus). The duration of the drug ejection usually lasted 8–10 min and the recording protocols were extended until the effect of the drug had disappeared (60 to 90 minutes approx.). The multibarrel assembly was positioned over the pial surface of the auditory cortex, forming a 30° angle with the horizontal plane towards the rostral direction, and advanced using a piezoelectric micromanipulator (Sensapex) until we observed a strong spiking activity synchronized with the train of search stimuli. Analog signals were digitalized with a RZ6 Multi I/O Processor, a RA16PA Medusa Preamplifier and a ZC16 headstage (TDT) at 12 kHz

675 sampling rate and amplified 251x. Neurophysiological signals for multiunit activity were
676 band-pass filtered between 0.5 and 4.5 kHz.

677 **Experimental Design and stimulation paradigms**

678 Sound stimuli were generated using the RZ6 Multi I/O Processor (TDT) and custom software
679 programmed with the OpenEx Suite (TDT) and MATLAB. Sounds were presented
680 monaurally through a speaker, in a close-field condition to the ear contralateral to the left
681 auditory cortex. We calibrated the speaker to ensure a flat spectrum up to ~75 dB SPL
682 between 0.5 and 44 kHz; the second and third harmonics were at least 40 dB lower than the
683 fundamental at the loudest output level for all the frequencies. The experimental stimuli were
684 pure tones in the range 0.5–44 kHz, with a duration of 75 ms, including 5 ms rise/fall ramps
685 presented at a rate of 4 stimuli/s. Once a suitable neuron was found, the frequency response
686 area (FRA) of the cell, i.e. the combination of frequencies and intensities capable of evoking a
687 suprathreshold response, was obtained automatically using a randomized paradigm that
688 presented tones between 0.5-44 kHz in 25 logarithmic steps, with intensities spaced by 10 dB
689 steps, from 0 to 70 dB SPL, at a repetition rate of 4/s. Based on this information, we selected a
690 pair of frequencies evoking similar responses at 10–30 dB above threshold. We used pure
691 tones at these frequencies as the stimuli in the oddball paradigm. Oddball sequences consisted
692 of frequently repeating stimuli (standard tones) which were pseudo-randomly interleaved with
693 rare events (deviant tones). Two oddball sequences with fixed parameters (400 trials each, 75
694 ms stimulus duration, 0.5 octaves frequency separation, 10% deviant probability, 250 ms
695 onset to onset, and a minimum of three standard tones before a deviant) were presented for
696 every pair of stimuli thus selected. In one of the sequences, the low frequency (*f1*) was the
697 "standard" and the high frequency (*f2*) was the "deviant," and in the other sequence their roles
698 were inverted. The order of presentation of these two sequences was randomized across sites.

In some cases, one or more extra pairs of stimuli were selected, and the oddball sequences were repeated with the new stimuli.

According to the predictive coding framework, mismatch responses like those obtained during an oddball paradigm can be divided in two components: repetition suppression, a reduction in the response caused by a repeated stimulus, and prediction error, an increased response caused by the violation of a regularity (Carbajal and Malmierca, 2018). In a subset of the experiments, we used control sequences to evaluate the separate contribution of repetition suppression and prediction error. Control sequences consisted of 10 tones evenly spaced by 0.5 octaves (same as in the oddball sequences), including the tones used in the oddball paradigm, and all stimuli at the same previously chosen sound level. Each control sequence lasted 400 trials, the duration of all stimuli was 75 ms and the presentation rate 4/s. We used two different control sequences, namely the many-standards and cascade sequences (Supplementary Figure 1). The many-standards control is the consecutive presentation of blocks of 10 tones randomly ordered within the block, each tone with a 10% probability of occurrence (Schroger and Wolff, 1996). In this sequence the tones are unpredictable, and it is not possible to establish a rule which could be used to predict the following tones. On the other hand, the cascade control consists of the regular presentation of the same 10 tones in ascending or descending frequency succession (Ruhnau et al., 2012). This sequence also avoids the effects of the repetition of a single stimulus, but in this case, it maintains a predictable context. Cascade sequences are considered a more rigorous control than many-standard sequences because like the oddball sequence, a regularity is established (Carbajal and Malmierca, 2018).

723 **Data analysis**

724 We calculated the bandwidth of the FRAs (Fig. 4) for each recorded unit by measuring the
725 width of the response area in octaves (relative to the low frequency border), at 10 and 30 dB
726 above minimum threshold (BW10 and BW30, respectively).

727 The degree of nMM was quantified by the common SSA index (CSI), reported previously
728 (Malmierca et al., 2009; Ulanovsky et al., 2004, 2003) . The CSI reflects the difference
729 between the neural responses to the deviant and standard stimuli, normalized to the total of
730 responses to both stimuli, and is defined as:

731 $$CSI = \frac{d(f_1) + d(f_2) - s(f_1) - s(f_2)}{d(f_1) + d(f_2) + s(f_1) + s(f_2)}$$

732 where $d(f_i)$ and $s(f_i)$ are responses to each frequency f_1 or f_2 when they were the deviant
733 (d) or standard (s) stimulus in the oddball paradigm, respectively.

734 Similarly, a frequency-specific SSA index (SI) was calculated for each of the frequencies
735 presented in an oddball paradigm, as:

736 $$SI = \frac{d(f) - s(f)}{d(f) + s(f)}$$

737 where $d(f)$ and $s(f)$ are responses to frequency f when it was the deviant (d) or standard (s)
738 stimulus in the oddball paradigm, respectively.

739 For the subset of experiments where we recorded the many-standards and cascade controls,
740 we compared the responses to the same physical stimulus when it took the role of a standard,
741 a deviant (ascending or descending, depending on whether the preceding standard was of
742 lower or higher frequency, respectively), or was part of a cascade sequence (matching the
743 ascending or descending condition of the corresponding deviant). Alongside the oddball
744 paradigm, we recorded responses of neurons to two cascade sequences (ascending and

descending), which consisted of 10 tones selected within the FRA presented in a predictable succession of increasing or decreasing frequencies. We did not include the many-standards control in these analyses because these experiments are time consuming and the need of holding the recording neuron for long enough before, during and after the drug injection. However, we have previously demonstrated that the many-standards and cascade controls responses were comparable, and the latter is considered to be more rigorous. (Casado-Román et al., 2019; Parras et al., 2017; Ruhnau et al., 2012; Valdés-Baizabal et al., 2019).

The responses of each neuron were normalized for each tested frequency as

$$Normalized\ Deviant = Deviant/N$$

$$Normalized\ Standard = Standard/N$$

$$Normalized\ Control = Control/N$$

where

$$N = \sqrt{Deviant^2 + Standard^2 + Control^2}$$

is the Euclidean norm of the vector defined by the deviant, standard and cascade responses, so that the normalized responses take values in the range 0–1.

With these normalized baseline-corrected spike counts, we next computed the indices of neuronal mismatch (iMM), repetition suppression (iRS), and prediction error (iPE) as:

$$iMM = Normalized\ Deviant - Normalized\ Standard$$

$$iRS = Normalized\ Control - Normalized\ Standard$$

$$iPE = Normalized\ Deviant - Normalized\ Control$$

765 Index values ranged between -1 and 1 and facilitated the quantitative decomposition of
766 neuronal mismatch into repetition suppression and prediction error since

767 $$iMM = iRS + iPE$$

768 Which is largely comparable to the CSI calculated for the oddball paradigm (Parras et al.,
769 2017). In order to determine a significant effect of the drugs on the CSI (Fig. 5a), we
770 calculated an empirical distribution of CSI values by performing 2000 bootstraps of the
771 responses to each standard or deviant stimulus for each neuron in the control condition, from
772 which we determined a 95% confidence interval (vertical lines in Fig. 5a). An effect was
773 considered significant at α=0.05 if the CSI during the drug condition fell beyond the limits of
774 the control CSI confidence interval (red dots in Fig. 5a). An equivalent approach was
775 followed for the SI values in Fig. 6a.

776 The area under the receiver operating characteristic (ROC) curve (AUC) was calculated using
777 the firing rates in response to deviant or standard stimuli as predictors (Figs 5d and 6c,d).
778 Mutual Information of the firing rates in response to deviant or standard stimuli was
779 calculated using the Information Breakdown Toolbox (Magri et al., 2009).

780 The confidence intervals for the variance of the different index distributions (Fig. 8), were
781 obtained by performing 1000 bootstraps.

782 Since parameters did not follow a normal distribution, non-parametric statistics were used:
783 Mann-Whitney (for independent data) or Wilcoxon Signed Rank test (for paired data).
784 Multiple comparisons were corrected using the Holm-Bonferroni approach. Unless stated
785 otherwise, all data are reported as mean ± SD. All of the data analyses were performed with
786 Sigma Plot v12.5 and MATLAB software, using the built-in functions, the Statistics and
787 Machine Learning toolbox, or custom scripts and functions developed in our laboratory.

788

Acknowledgments: We thank Drs. Francisco Garcia-Rosales and Julio Hechavarria for their advice in the mutual information analysis and Drs. Ryszard Auksztulewicz, Yaneri A. Ayala, Donald Caspary, Diego Contreras, Karl Friston, Lauren Harms and Marina Picciotto for their constructive criticisms on a previous version. Finantial support was provided by the Spanish Agencia Estatal de Investigación grant (AEI), PID2019-104570RB-I00 (MSM, ABLR); the European Union's Horizon 2020 grant agreement No 952378- BrainTwin (MSM, DPG, ABLR) and the Foundation Ramón Areces grant CIVP20A6616 (MSM and DPG).

Competing interests: No competing interests declared

REFERENCES

Auksztulewicz R, Friston K. 2016. Repetition suppression and its contextual determinants in predictive coding. *Cortex* **80**:125–140. doi:10.1016/j.cortex.2015.11.024

Auksztulewicz R, Friston KJ, Nobre AC. 2017. Task relevance modulates the behavioural and neural effects of sensory predictions. *PLoS Biol* **15**:e2003143. doi:10.1371/journal.pbio.2003143

Auksztulewicz R, Rajendran VG, Peng F, Schnupp JWH, Harper NS. 2023. Omission responses in local field potentials in rat auditory cortex. *BMC Biol* **21**:130. doi:10.1186/s12915-023-01592-4

Auksztulewicz R, Schwiedrzik CM, Thesen T, Doyle W, Devinsky O, Nobre AC, Schroeder CE, Friston KJ, Melloni L. 2018. Not All Predictions Are Equal: "What" and "When" Predictions Modulate Activity in Auditory Cortex through Different Mechanisms. *J Neurosci* **38**:8680–8693. doi:10.1523/JNEUROSCI.0369-18.2018

Ayala YA, Malmierca MS. 2015. Cholinergic Modulation of Stimulus-Specific Adaptation in the Inferior Colliculus. *J Neurosci* **35**:12261–12272. doi:10.1523/JNEUROSCI.0909-15.2015

Bastos AM, Usrey WM, Adams RA, Mangun GR, Fries P, Friston KJ. 2012. Canonical Microcircuits for Predictive Coding. *Neuron* **76**:695–711. doi:10.1016/j.neuron.2012.10.038

Batista-Brito R, Zagha E, Ratliff JM, Vinck M. 2018. Modulation of cortical circuits by top-down processing and arousal state in health and disease. *Curr Opin Neurobiol* **52**:172–181. doi:10.1016/j.conb.2018.06.008

Carbajal G V., Malmierca MS. 2020. Novelty Processing in the Auditory System: Detection, Adaptation or Expectation? In: Fritzsch B, Gothe B, editors. The Senses: A Comprehensive Reference. Elsevier. pp. 749–776. doi:10.1016/B978-0-12-809324-5.24154-0

Carbajal G V., Malmierca MS. 2018. The Neuronal Basis of Predictive Coding Along the Auditory Pathway: From the Subcortical Roots to Cortical Deviance Detection. *Trends Hear* **22**:233121651878482. doi:10.1177/2331216518784822

Casado-Román L, Carbajal G V., Pérez-González D, Malmierca MS. 2020. Prediction error signaling explains neuronal mismatch responses in the medial prefrontal cortex. *PLoS Biol* **18**:e3001019. doi:10.1371/journal.pbio.3001019

Casado-Román L, Pérez-González D, Malmierca MS. 2019. Prediction errors explain mismatch signals of neurons in the medial prefrontal cortex. *bioRxiv* 778928. doi:10.1101/778928

Chavez C, Zaborszky L. 2017. Basal forebrain cholinergic-auditory cortical network: Primary versus nonprimary auditory cortical areas. *Cereb Cortex* **27**:2335–2347. doi:10.1093/cercor/bhw091

Chen I-W, Helmchen F, Lütcke H. 2015. Specific Early and Late Oddball-Evoked Responses in Excitatory and Inhibitory Neurons of Mouse Auditory Cortex. *Soc Neurosci*. doi:10.1523/JNEUROSCI.2240-15.2015

Colangelo C, Shichkova P, Keller D, Markram H, Ramaswamy S. 2019. Cellular, Synaptic and Network Effects of Acetylcholine in the Neocortex. *Front Neural Circuits* **13**:24. doi:10.3389/fncir.2019.00024

Dalley JW, Cardinal RN, Robbins TW. 2004. Prefrontal executive and cognitive functions in rodents: neural and neurochemical substrates. *Neurosci Biobehav Rev*

28:771–784. doi:10.1016/j.neubiorev.2004.09.006
Dasgupta R, Seibt F, Beierlein M. 2018. Synaptic release of acetylcholine rapidly suppresses cortical activity by recruiting muscarinic receptors in layer 4. *J Neurosci* **38**:5338–5350. doi:10.1523/JNEUROSCI.0566-18.2018
Edeline JM. 2012. Beyond traditional approaches to understand the functional role of neuromodulators in sensory cortices. *Front Behav Neurosci* **6**:1–14. doi:10.3389/fnbeh.2012.00045
Eggermann E, Feldmeyer D. 2009. Cholinergic filtering in the recurrent excitatory microcircuit of cortical layer 4. *Proc Natl Acad Sci U S A* **106**:11753–11758. doi:10.1073/pnas.0810062106
Feldman H, Friston KJ. 2010. Attention, Uncertainty, and Free-Energy. *Front Hum Neurosci* **4**:215. doi:10.3389/fnhum.2010.00215
Franklin NT, Frank MJ. 2015. A cholinergic feedback circuit to regulate striatal population uncertainty and optimize reinforcement learning. *Elife* **4**:1–29. doi:10.7554/eLife.12029
Friston K. 2023. Computational psychiatry: from synapses to sentience. *Mol Psychiatry* **28**:256–268. doi:10.1038/s41380-022-01743-z
Friston K. 2018. Does predictive coding have a future? *Nat Neurosci* **21**:1019–1021. doi:10.1038/s41593-018-0200-7
Friston K. 2008. Hierarchical Models in the Brain. *Cit Frist K* **4**:1000211. doi:10.1371/journal.pcbi.1000211
Friston K, Kiebel S. 2009. Cortical circuits for perceptual inference. *Neural Networks* **22**:1093–1104. doi:10.1016/j.neunet.2009.07.023
Friston KJ. 2005. A theory of cortical responses. *Philos Trans R Soc B Biol Sci* **360**:815–836. doi:10.1098/rstb.2005.1622
Froemke RC, Merzenich MM, Schreiner CE. 2007. A synaptic memory trace for cortical receptive field plasticity. *Nature* **450**:425–429. doi:10.1038/nature06289
Fu Y, Tucciarone JM, Espinosa JS, Sheng N, Darcy DP, Nicoll RA, Huang ZJ, Stryker MP. 2014. A cortical circuit for gain control by behavioral state. *Cell* **156**:1139–1152. doi:10.1016/j.cell.2014.01.050
Games KD, Winer JA. 1988. Layer V in rat auditory cortex: Projections to the inferior colliculus and contralateral cortex. *Hear Res* **34**:1–25. doi:10.1016/0378-5955(88)90047-0
Harms L, Parras GG, Michie PT, Malmierca MS. 2020. The Role of Glutamate Neurotransmission in Mismatch Negativity (MMN), A Measure of Auditory Synaptic Plasticity and Change-detection. *Neuroscience*. doi:10.1016/j.neuroscience.2020.01.046
Hasselmo ME. 1999. Neuromodulation: Acetylcholine and memory consolidation. *Trends Cogn Sci*. doi:10.1016/S1364-6613(99)01365-0
Hasselmo ME, Giocomo LM. 2006. Cholinergic Modulation of Cortical Function. *J Mol Neurosci* **30**:133–136. doi:10.1385/JMN:30:1:133
Hasselmo ME, Sarter M. 2011. Modes and models of forebrain cholinergic neuromodulation of cognition. *Neuropsychopharmacology*. doi:10.1038/npp.2010.104
Irvine DRF. 2018a. Auditory perceptual learning and changes in the conceptualization of auditory cortex. *Hear Res*. doi:10.1016/j.heares.2018.03.011
Irvine DRF. 2018b. Plasticity in the auditory system. *Hear Res*. doi:10.1016/j.heares.2017.10.011
Ishishita Y, Kunii N, Shimada S, Ibayashi K, Tada M, Kirihara K, Kawai K, Uka T, Kasai K, Saito N. 2019. Deviance detection is the dominant component of auditory

contextual processing in the lateral superior temporal gyrus: A human ECoG study. *Hum Brain Mapp* **40**:1184–1194. doi:10.1002/hbm.24438
Kamke MR, Brown M, Irvine DRF. 2005. Basal forebrain cholinergic input is not essential for lesion-induced plasticity in mature auditory cortex. *Neuron* **48**:675–686. doi:10.1016/j.neuron.2005.09.014
Keller GB, Mrsic-Flogel TD. 2018. Predictive Processing: A Canonical Cortical Computation. *Neuron* **100**:424–435. doi:10.1016/j.neuron.2018.10.003
Kilgard MP, Merzenich MM. 1998. Cortical Map Reorganization Enabled by Nucleus Basalis Activity. *Science (80-)* **279**:1714–1718. doi:10.1126/science.279.5357.1714
Kok P, Jehee JFM, de Lange FP. 2012a. Less Is More: Expectation Sharpens Representations in the Primary Visual Cortex. *Neuron* **75**:265–270. doi:10.1016/j.neuron.2012.04.034
Kok P, Rahnev D, Jehee JFM, Lau HC, de Lange FP. 2012b. Attention Reverses the Effect of Prediction in Silencing Sensory Signals. *Cereb Cortex* **22**:2197–2206. doi:10.1093/cercor/bhr310
Lao-Rodríguez AB, Przewrocki K, Pérez-González D, Alishbayli A, Yilmaz E, Malmierca MS, Englitz B. 2023. Neuronal responses to omitted tones in the auditory brain: A neuronal correlate for predictive coding. *Sci Adv* **9**:eabq8657. doi:10.1126/sciadv.abq8657
Lucas-Meunier E, Fossier P, Baux G, Amar M. 2003. Cholinergic modulation of the cortical neuronal network. *Pflugers Arch* **446**:17–29. doi:10.1007/s00424-002-0999-2
Ma X, Suga N. 2005. Long-term cortical plasticity evoked by electric stimulation and acetylcholine applied to the auditory cortex. *Proc Natl Acad Sci U S A* **102**:9335–9340. doi:10.1073/pnas.0503851102
Magri C, Whittingstall K, Singh V, Logothetis NK, Panzeri S. 2009. A toolbox for the fast information analysis of multiple-site LFP , EEG and spike train recordings. *BMC Neurosci* **10**. doi:10.1186/1471-2202-10-81
Malmierca MS. 2015. Auditory System In: Paxinos G, editor. The Rat Nervous System. Elsevier - Academic Press. pp. 865–946.
Malmierca MS, Cristaudo S, Pérez-González D, Covey E. 2009. Stimulus-specific adaptation in the inferior colliculus of the anesthetized rat. *J Neurosci* **29**:5483–5493. doi:10.1523/JNEUROSCI.4153-08.2009
Marshall L, Mathys C, Ruge D, de Berker AO, Dayan P, Stephan KE, Bestmann S. 2016. Pharmacological Fingerprints of Contextual Uncertainty. *PLoS Biol* **14**. doi:10.1371/journal.pbio.1002575
Martins ARO, Froemke RC. 2015. Coordinated forms of noradrenergic plasticity in the locus coeruleus and primary auditory cortex. *Nat Neurosci* **18**:1483–1492. doi:10.1038/nn.4090
Mesulam M-M. 2013. Cholinergic circuitry of the human nucleus basalis and its fate in Alzheimer's disease. *J Comp Neurol* **521**:4124–4144. doi:10.1002/cne.23415
Metherate R. 2011. Functional connectivity and cholinergic modulation in auditory cortex. *Neurosci Biobehav Rev* **35**:2058–2063. doi:10.1016/j.neubiorev.2010.11.010
Metherate R, Cox CL, Ashe JH. 1992. Cellular bases of neocortical activation: Modulation of neural oscillations by the nucleus basalis and endogenous acetylcholine. *J Neurosci* **12**:4701–4711. doi:10.1523/jneurosci.12-12-04701.1992
Minces V, Pinto L, Dan Y, Chiba AA. 2017. Cholinergic shaping of neural correlations. *Proc Natl Acad Sci U S A* **114**:5725–5730. doi:10.1073/pnas.1621493114

Moran RJ, Campo P, Symmonds M, Stephan KE, Dolan RJ, Friston KJ. 2013. Free energy, precision and learning: The role of cholinergic neuromodulation. *J Neurosci* **33**:8227–8236. doi:10.1523/JNEUROSCI.4255-12.2013

Motts SD, Schofield BR. 2009. Sources of cholinergic input to the inferior colliculus. *Neuroscience* **160**:103–114. doi:10.1016/j.neuroscience.2009.02.036

Muñoz W, Rudy B. 2014. Spatiotemporal specificity in cholinergic control of neocortical function. *Curr Opin Neurobiol* **26**:149–160. doi:10.1016/j.conb.2014.02.015

Nelken I. 2014. Stimulus-specific adaptation and deviance detection in the auditory system: experiments and models. *Biol Cybern*. doi:10.1007/s00422-014-0585-7

Netser S, Zahar Y, Gutfreund Y. 2011. Stimulus-specific adaptation: Can it be a neural correlate of behavioral habituation? *J Neurosci* **31**:17811–17820. doi:10.1523/JNEUROSCI.4790-11.2011

Nieto-Diego J, Malmierca MS. 2016. Topographic Distribution of Stimulus-Specific Adaptation across Auditory Cortical Fields in the Anesthetized Rat. *PLoS Biol* **14**:1–30. doi:10.1371/journal.pbio.1002397

Ogawa H, Oka K. 2015. Direction-Specific Adaptation in Neuronal and Behavioral Responses of an Insect Mechanosensory System. *Soc Neurosci*. doi:10.1523/JNEUROSCI.1378-15.2015

Parr T, Friston KJ. 2017. Uncertainty, epistemics and active inference. *J R Soc Interface* **14**:20170376. doi:10.1098/rsif.2017.0376

Parras GG, Nieto-Diego J, Carbajal G V., Valdés-Baizabal C, Escera C, Malmierca MS. 2017. Neurons along the auditory pathway exhibit a hierarchical organization of prediction error. *Nat Commun* **8**. doi:10.1038/s41467-017-02038-6

Parras GG, Valdés-Baizabal C, Harms L, Michie PT, Malmierca MS. 2020. The effect of NMDA-R antagonist, MK-801, on neuronal mismatch along the rat auditory thalamocortical pathway. *Sci Rep* **10**:12391. doi:10.1038/s41598-020-68837-y

Paxinos G, Watson C, Diego S, Boston L, York N. 1997. The Rat Brainin Stereotaxic Coordinates Academic Press.

Picciotto MR, Higley MJ, Mineur YS. 2012. Acetylcholine as a Neuromodulator: Cholinergic Signaling Shapes Nervous System Function and Behavior. *Neuron* **76**:116–129. doi:10.1016/j.neuron.2012.08.036

Pinto L, Goard MJ, Estandian D, Xu M, Kwan AC, Lee SH, Harrison TC, Feng G, Dan Y. 2013. Fast modulation of visual perception by basal forebrain cholinergic neurons. *Nat Neurosci* **16**:1857–1863. doi:10.1038/nn.3552

Polack PO, Friedman J, Golshani P. 2013. Cellular mechanisms of brain state-dependent gain modulation in visual cortex. *Nat Neurosci* **16**:1331–1339. doi:10.1038/nn.3464

Polley DB, Read HL, Storace DA, Merzenich MM. 2007. Multiparametric auditory receptive field organization across five cortical fields in the albino rat. *J Neurophysiol* **97**:3621–3638. doi:10.1152/jn.01298.2006

Puckett AC, Pandya PK, Moucha R, Dai W, Kilgard MP. 2007. Plasticity in the Rat Posterior Auditory Field Following Nucleus Basalis Stimulation. *J Neurophysiol* **98**:253–265. doi:10.1152/jn.01309.2006

Qi G, Feldmeyer D. 2022. Cell-Type Specific Neuromodulation of Excitatory and Inhibitory Neurons via Muscarinic Acetylcholine Receptors in Layer 4 of Rat Barrel Cortex. *Front Neural Circuits* **16**:1–16. doi:10.3389/fncir.2022.843025

Ruhnau P, Herrmann B, Schröger E. 2012. Finding the right control: The mismatch negativity under investigation. *Clin Neurophysiol* **123**:507–512. doi:10.1016/j.clinph.2011.07.035

Sarter M, Givens B, Bruno JP. 2001. The cognitive neuroscience of sustained attention: Where top-down meets bottom-up. *Brain Res Rev*. doi:10.1016/S0165-0173(01)00044-3

Schöbi D, Homberg F, Frässle S, Endepols H, Moran RJ, Friston KJ, Tittgemeyer M, Heinzle J, Stephan KE. 2021. Model-based prediction of muscarinic receptor function from auditory mismatch negativity responses. *Neuroimage* **237**. doi:10.1016/j.neuroimage.2021.118096

Schroger E, Wolff C. 1996. Mismatch response of the human brain to changes in sound location. *Neuroreport* **7**:3005–3008.

Shipp S. 2016. Neural elements for predictive coding. *Front Psychol* **7**:1792. doi:10.3389/fpsyg.2016.01792

Spratling MW. 2008. Reconciling predictive coding and biased competition models of cortical function. *Front Comput Neurosci* **2**:4. doi:10.3389/neuro.10.004.2008

Thiele A, Bellgrove MA. 2018. Neuromodulation of Attention. *Neuron*. doi:10.1016/j.neuron.2018.01.008

Ulanovsky N, Las L, Farkas D, Nelken I. 2004. Multiple time scales of adaptation in auditory cortex neurons. *J Neurosci* **24**:10440–10453.

Ulanovsky N, Las L, Nelken I. 2003. Processing of low-probability sounds by cortical neurons. *Nat Neurosci* **6**:391–398. doi:10.1038/nn1032

Valdés-Baizabal C, Carbajal G V., Pérez-González D, Malmierca MS. 2019. Dopamine gates prediction error forwarding in the cortices of the inferior colliculus. *bioRxiv* 824656. doi:10.1101/824656

von der Behrens W, Bäuerle P, Kössl M, Gaese BH. 2009. Correlating stimulus-specific adaptation of cortical neurons and local field potentials in the awake rat. *J Neurosci* **29**:13837–13849. doi:10.1523/JNEUROSCI.3475-09.2009

Vossel S, Weidner R, Driver J, Friston KJ, Fink GR. 2012. Deconstructing the architecture of dorsal and ventral attention systems with dynamic causal modeling. *J Neurosci* **32**:10637–10648. doi:10.1523/JNEUROSCI.0414-12.2012

Weinberger NM. 2004. Specific long-term memory traces in primary auditory cortex. *Nat Rev Neurosci* **5**:279–290. doi:10.1038/nrn1366

Yarden TS, Mizrahi A, Nelken I. 2022. Context-Dependent Inhibitory Control of Stimulus-Specific Adaptation. *J Neurosci* **42**:4629–4651. doi:10.1523/JNEUROSCI.0988-21.2022

Yon D, Frith CD. 2021. Precision and the Bayesian brain. *Curr Biol* **31**:R1026–R1032. doi:10.1016/j.cub.2021.07.044

Yu AJ, Dayan P. 2005. Uncertainty, Neuromodulation, and Attention. *Neuron* **46**:681–692. doi:10.1016/j.neuron.2005.04.026

Yu AJ, Dayan P. 2002. Acetylcholine in cortical inference. *Neural Networks* **15**:719–730. doi:10.1016/S0893-6080(02)00058-8

Zaborszky L, Hoemke L, Mohlberg H, Schleicher A, Amunts K, Zilles K. 2008. Stereotaxic probabilistic maps of the magnocellular cell groups in human basal forebrain. *Neuroimage* **42**:1127–1141. doi:10.1016/j.neuroimage.2008.05.055

SUPPLEMENTARY FIGURES

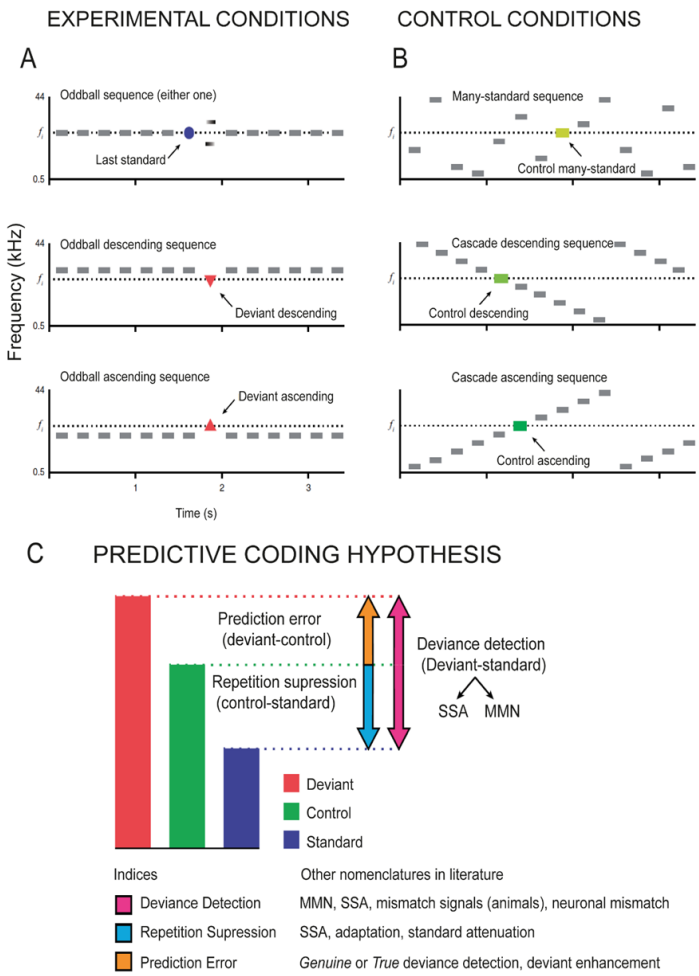

Supplementary Figure 1. Experimental paradigms and Interpretation of the control conditions. (A) *Classic oddball paradigm, showing three possible experimental conditions for a given f_i target tone: STD (blue circle, top panel), DEV descending (red triangle pointing downwards, middle panel) and DEV ascending (red triangle pointing upwards, bottom panel).* ***(B)*** *CTR sequences highlighting the f_i target tone. In the many-standard control (very light green rectangle), the target tone is embedded within a random succession of equiprobable tones, making it impossible for the system to establish a precise prediction or accurately encode a regularity. Two versions of the cascade sequence: Cascade descending sequence (light green rectangle) and Cascade ascending sequence (dark green rectangle) are compared with the DEV descending and ascending, respectively. In both versions, the target tone f_i is embedded in a regular succession of equiprobable tones in both cases. This allows the system to generate a precise prediction or encode that regularity, because it is not violated by the appearance of the target tone f_i, as opposed to DEV.* ***(C)*** *Decomposition of the differential response by means of the control condition (green bar), yielding indices of mismatch (iMM, in magenta), prediction error (iPE, in orange) and repetition suppression (iRS, in cyan). Modified after Carbajal and Malmierca* (2020, 2018).